Stanford University
Basin and Petroleum System Modeling
12th Annual Industrial Affiliates Meeting

November 11-13, 2019
Stanford, California

Meeting Guide compiled by
Allegra Hosford Scheirer and Cerise Burns

Field Trip Guide by
Allegra Hosford Scheirer and Les Magoon
http://bpsm.stanford.edu

2019 BPSM Industrial Affiliates

Aker BP
Bureau of Energy Ocean Management
ConocoPhillips
Equinor
ExxonMobil
JOGMEC
Oxy (formerly Anadarko)
Petrobras
Total Energy

Schedule of Events

Monday, 11/11/19, 5:30-7:30 p.m.	Icebreaker at Vina Enoteca, Palo Alto
Tuesday, 11/12/19, 8:30 a.m.-5:00 p.m.	Oral and poster session at Stanford University Faculty Club
Tuesday, 11/12/19, 6:00-9:00 p.m.	Group dinner at Terrain Cafe, Palo Alto
Wednesday, 11/13/19, 8:00 a.m.-5:00 p.m.	Field trip to Black Diamond Mines, Antioch

November 12, 2019: Oral Session Agenda

Morning

9:00 a.m.	Steve Graham, Introduction

Pore Pressure, Faults, Uncertainty and Sensitivity Analysis in Petroleum Systems

9:20 a.m.	Anshuman Pradhan, Pore pressure uncertainty quantification with constraints from basin modeling and seismic imaging
9:45 a.m.	Best Chaipornkaew, Basin-scale natural fracturing and its impact on modeling stress and pore pressure evolution
10:15-10:30 a.m.	Coffee break
10:30 a.m.	Marcelo Silka, Sensitivity analysis of migration through faults
10:50 a.m.	Anatoly Aseev, Understanding of impact of fault properties and reservoir heterogeneity on petroleum systems modeling, South Viking Graben, North Sea
11:10 a.m.	Tanvi Chheda, Bayesian Networks to use field data for reducing uncertainty in 3D basin model of the Jeanne d'Arc Basin
11:35 p.m.	Tapan Mukerji, Quantitative seismic interpretation in organic-rich mudrocks: Shublik Formation, North Slope, Alaska
11:50-1:00 p.m.	Lunch

Afternoon

Gas Hydrate Petroleum Systems

1:00 p.m.	Zack Burton, Inventory of organic properties of shallow sediments with application to basin modeling of gas hydrate systems
1:25 p.m.	Laura Dafov, Three-dimensional basin model of Terrebonne Basin, Gulf of Mexico gas hydrate system

Modeling Carbonates in Petroleum Systems

1:50 p.m.	Pulkit Singh, Rule based modeling of attached carbonate platforms
2:10 p.m.	Xiaowei Li, Predicting depositional interparticle porosity of oolite using ooid size

Basin Modeling and Geochemistry

2:30 p.m.	Mei Mei, Modeling petroleum expulsion and retention from source rocks within the Vaca Muerta Formation, Neuquén Basin, Argentina
2:55-3:10 p.m.	Coffee break
3:15 p.m.	Will Thompson-Butler, Basin and petroleum system modeling in the Middle Magdalena Valley, Colombia
3:45 p.m.	Josué Fonseca, Introduction
4:00 p.m.	Allegra Hosford Scheirer, Quantitative evaluation rules for programmed pyrolysis data greatly improve their reliability
4:25 p.m.	Les Magoon, Preparation for field trip to Black Diamond Mine Regional Preserve

Evening

6:00-9:00 p.m.	Group Dinner at Terrain Café, Stanford Shopping Center, 180 El Camino Real #1301, Palo Alto, CA 94304

2019 Meeting Attendees

Attendee	Affiliate Organization
Than Tin Aung	JOGMEC
Peder Aursand	Aker BP
Silvana Barbanti	Biomarker Technologies Inc.
Mike Bidgood	Suncor Energy
Stephen Anthony ("Stoney") Clark	Equinor
John Cody	Equinor
Gabe Creason	National Energy Technology Laboratory
Jose Alberto De Araujo	Petrobras
Shuichi Desaki	INPEX
Tim Diggs	Aramco Services Company
François Gelin	Total
Toshinori Imai	JOGMEC
Sabrina Innocenti	ExxonMobil
Marek Kacewicz	Chevron
Benjamin Kirkland	CNOOC International
Alexandros Konstantinou	ExxonMobil
Cíntia Lima	Petrobras
Eric Michael	ConocoPhillips
J. "Mike" Moldowan	Biomarker Technologies Inc.
Ko Nifuku	INPEX
Stephen Palmes	BOEM
Ken Peters	Schlumberger and Adjunct Professor, Stanford
Kenneth Petersen	Hess Corporation
Dominic Smith	BOEM
Kevin Smith	BOEM
Ye Wang	ConocoPhillips
Johannes Wendebourg	Total
Lauren Zeigler	BOEM

Stanford Students	Stanford Students	Stanford Scientists
Anatoly Aseev	Anshuman Pradhan	Alan Burnham
Zachary Burton	Marcelo Silka	Nadar Dutta
Laainam "Best" Chaipornkaew	Pulkit Singh	Steve Graham
Tanvi Chheda	William Thompson-Butler	Allegra Hosford Scheirer
Laura Dafov		Yanran Huang (Visiting)
Josue Fonesca		Les Magoon
Xiaowei Li		Tapan Mukerji
Mei Mei (Postdoctoral Scholar)		Jonathan Payne

2019 Meeting Abstracts Follow

PORE PRESSURE UNCERTAINTY QUANTIFICATION WITH CONSTRAINTS FROM BASIN MODELING AND SEISMIC IMAGING

Anshuman Pradhan[1*], Nader C. Dutta[2], Allegra Hosford Scheirer[3], & Tapan Mukerji[1]
[1]Department of Energy Resources Engineering, [2]Department of Geophysics, [3]Department of Geological Sciences
Stanford University, Stanford, CA
[*]pradhan1@stanford.edu

Abstract

We present a methodology for pore pressure modeling under uncertainty that incorporates information regarding the geological history of the basin, rock physics, drilling, and seismic data. In particular, our approach relies on linking P-wave velocity models to the basin modeling outputs of porosity, mineral volume fractions and pore pressure through rock physics models (**Figure 1**). We account for geological uncertainty by defining prior probability distributions on uncertain parameters and performing Monte Carlo basin simulations. We perform probabilistic calibration of the basin model outputs by defining data likelihood distributions to represent well data uncertainty. We employ seismic imaging constraints by performing rock physics modeling to obtain multiple velocity realizations, which are subsequently used in multiple seismic depth migrations. We present an approximate Bayesian inference framework which facilitates updating pore pressure uncertainty by conditioning to both well and seismic data. We apply our methodology in 2D to a real field case from Northern Gulf of Mexico (**Figure 2**). In **Figure 3**, the initial pore pressure uncertainty at different locations in our basin is presented. We also show how our integrated workflow is effective in updating pore pressure uncertainty after sequential conditioning to well and seismic data. It can be seen that conditioning to seismic data assigns greater probability of the existence of overpressured zones in the basin. Our workflow may also be used to constrain the spatial pore pressure uncertainty constrained to well and seismic data (**Figure 4**) where we estimate the mean pore pressure cross section and corresponding standard deviation.

Figures

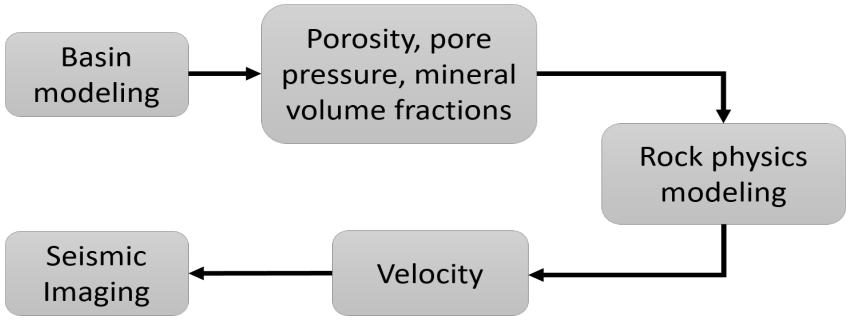

Figure 1. The integrated workflow used in this paper.

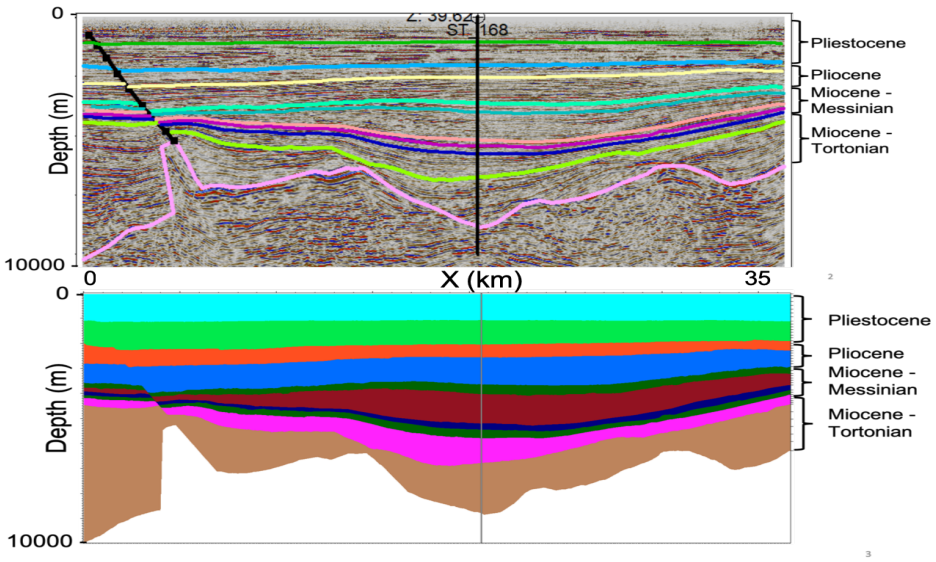

Figure 2. The depth migrated seismic section for which we present our analysis and interpretations of key geologic horizons. (Bottom) Corresponding structural model of the basin. The cross section is located in a north-central Gulf of Mexico basin off the coast of Louisiana.

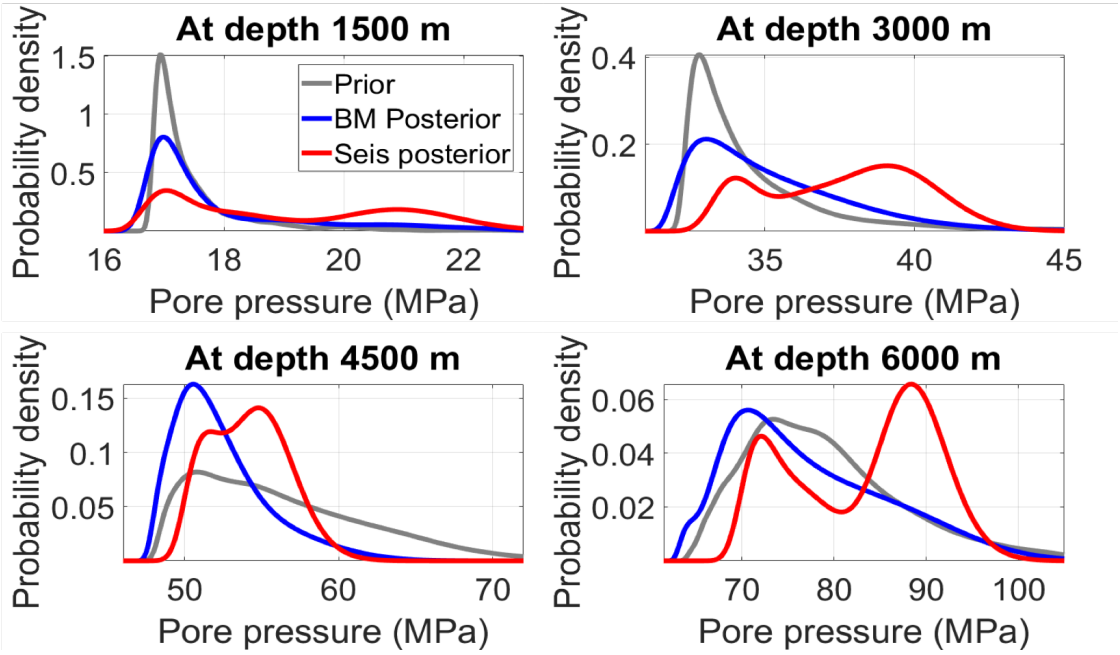

Figure 3. Estimates of pore pressure uncertainty estimated at x location of 15 km and at depths listed on top of each plot. Shown in gray is the prior uncertainty on the pore pressure and updated posterior distributions after constraining to basin modeling calibration data (blue) and seismic kinematic information (red).

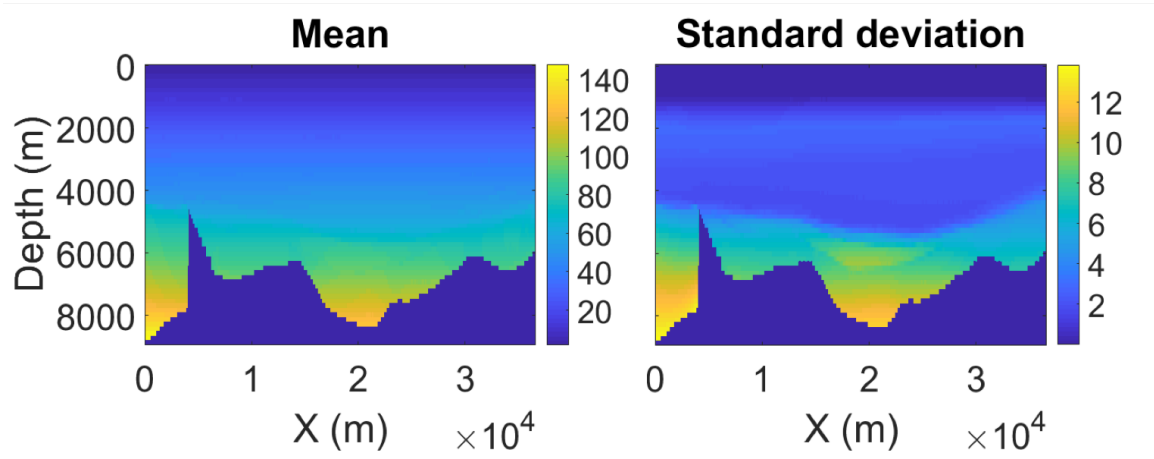

Figure 4. Posterior mean and standard deviation for pore pressure (in MPa) estimated using proposed workflow.

Acknowledgments

We thank Huy Q. Le and Prof. Biondo Biondi for their technical contributions with regards to the seismic imaging parts of proposed workflow and Schlumberger for PetroMod software.

BASIN-SCALE INELASTIC DEFORMATION: PORE PRESSURE AND STRESS IMPLICATIONS

Laainam (Best) Chaipornkaew[1,*], Marek Kacewicz[2], and Pete Lovely[2]
[1]*Department of Geological Sciences, Stanford University, Stanford, CA*
[2]*Chevron Energy Technology Company, Houston, Texas*
[*]bestc@stanford.edu
Abstract originally from: EAGE Annual Conference and Exhibition 2019

Introduction

Most sedimentary rocks experience some form of inelastic deformation, such as compaction under increased confining pressure, which may be enhanced by horizontal stresses at convergent margins. The behaviors of inelastic deformation and its impact on stress and pressure evolution is not well understood. Recent studies attempt to incorporate more realistic deformation for fractured and porous rocks via laboratory experiments and numerical simulations (Nicksiar and Martin, 2013; Rutqvist et al., 2002; Sone and Zoback, 2014; Wei and Anand, 2008). However, existing works do not emphasize inelastic deformation at the basin-scale or through geologic time.

Basin modeling accounts for the evolution of stress and pore pressure in sedimentary basins through geologic time. This is a more complete approach than other techniques that only consider in-situ stress conditions such as seismic-derived pore pressure or "static" mechanical earth models. However, several published studies using basin modeling techniques in structurally complex regions show inaccurate pressure predictions (Neumaier et al., 2014; Burgreen-Chan et al., 2016). This is typically due to elastic assumptions and lack of non-vertical deformation and stress.

This work uses an evolutionary geomechanical approach to basin modeling that represents inelastic deformation in response to the full stress tensor (Obradors-Prats 2016). The focus is to model seals with evolving properties as a function of stress and fracture formation. We use a synthetic model to investigate basin-scale effects of fracturing on fluid flow and pore pressure evolution. The model captures fracture opening, closing, and potential reactivation in response to mechanical criteria (**Figure 1**) as well as the system response when tectonic shortening is present.

Model Design

The synthetic framework is motivated by the Offshore East Coast Basin of New Zealand, an underexplored petroleum system with complex deformation and pressure history. We opt for a model with simplified, synthetic geometry because the inputs are known and outputs are fully predictable. The model allows introducing fracture mechanisms and tectonic effects and tracks pressure response. Overpressure conditions

are generated by rapid sedimentation of low permeability shales over an anticline with a layer of high-permeability sand (**Figure 2**).

Fracturing Criteria

A workflow is developed using the finite element code ParaGeo (Crook, 2013). This evolutionary geomechanical basin model uses a critical state poroelastoplastic constitutive formulation that accommodates compaction and shear dilatancy and is able to handle large strain accumulated through geologic time (Obradors-Prats et al., 2016). Fracturing occurs only when pressure and stress criteria are satisfied, leading to enhanced fluid flow modelled by permeability multiplier (**Figure 3**).

Results

We are able to model realistic mechanical behaviors of low-permeability shales in relation to compaction, overpressure conditions, fracturing, and tectonic shortening. Fluid flow, pressure, and stress evolution influence fracture generation and subsequent deactivation due to pressure dissipation (**Figure 1**). We showcase two examples, without and with tectonic shortening.

Example 1: Fracturing without Tectonic Loading

We tested three scenarios to highlight the effects of fracturing on fluid flow and pressure fields (**Figure 4**). When fracturing is not incorporated (A), pressure prediction is only varied along depth with unrealistic homogenous pressure distribution across sand and shale lithologies. When fractures remain open after being activated (B), preferred flow orientation is very different from a comparable model that assumes dynamic fractures (C), in which fracture permeability is reduced as pressure dissipates and effective stress increases. Flow (brown arrows) through supposedly "inactive" fractures (in B) leads to more intense pressure dissipation than compared to the dynamic fracture scenario.

Example 2: Fracturing with Tectonic Shortening

In addition, this example incorporates the effects of tectonic shortening to understand the relationship between fracturing and the evolving fluid flow and pressure. The model is built with a fixed-based and rolling-base boundary condition, similar to a convergent margin setting such as the Hikurangi Trough (**Figure 2**). Shortening-enhanced compaction not only increases pore pressure but also increases total horizontal stress, two processes that have competing effects on fracture generation. The tectonic component also innately introduces asymmetry to structural geometry and preferred flow orientation, leading to asymmetry in fracture locality and pressure distribution. This is a product of tectonic loading and asymmetry of the base boundary conditions. Lastly, pressure evolution controls fracture deactivation and reactivation even more evidently with shortening. An example of asymmetric development of fractures and evolution of overpressure is presented in **Figure 5**. Following further syntectonic sedimentation and hiatus steps, the present-day overpressure condition demonstrates that overpressure

prediction might exhibit substantial errors if shortening and fracturing are not properly considered.

Conclusions

Though we study a simplified, synthetic geometry, our model results are geologically realistic and insightful. An example without tectonic loading is able to generate a dissipation mechanism via natural fracturing at the location where pressure and stress condition exceed the elastic limit. An example with tectonic shortening predicts a consistent deformation zone and preferred flow orientation in relation to compressive forces. Abundant fracturing and deformation zones are also observed across the Hikurangi Trough, which are the focus for gas hydrate migration pathway (Barnes et al., 2010). Preferred flow orientation (west to east) results in fluid migration away from the subduction zone to onshore New Zealand, as supported by hydrocarbon seeps found along the coast of the East Coast Basin.

Fractures enhance communication of pore pressure leading to a dynamic relation between fracture state, fluid flow, and pore pressure. The ability to model timing and location of fracturing can improve basin model results related to pore pressure and stress conditions, which has direct implications for hydrocarbon migration, seal and reservoir quality. This is an important first step in forward modeling stress and pressure history in a complex region influenced by fractures and horizontal shortening.

Acknowledgments

The authors thank Chevron Energy Technology Company and Three Cliffs Geomechanical Analysis Ltd. for access to *ParaGeo* software and for permission to present this work. Funding and participation in the basin-scale inelastic deformation research is made possible through the support of the Stanford Basin and Petroleum System Modeling Group with essential advancement of fracture modeling via evolutionary geomechanical approach through an internship at Chevron Energy Technology Company.

Figures

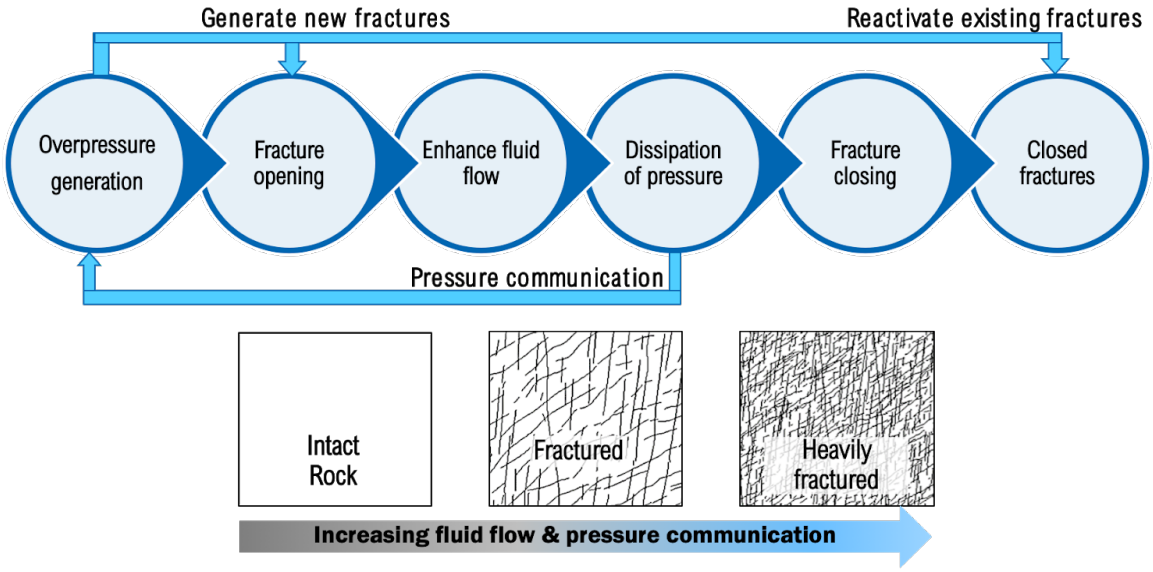

Figure 1. Diagram illustrates the relationship between pressure, fluid flow, and fractures. We modeled these processes and the interaction between them. Fracture states (open/ closed) in our model are adjusted by permeability multipliers applied to rock matrix.

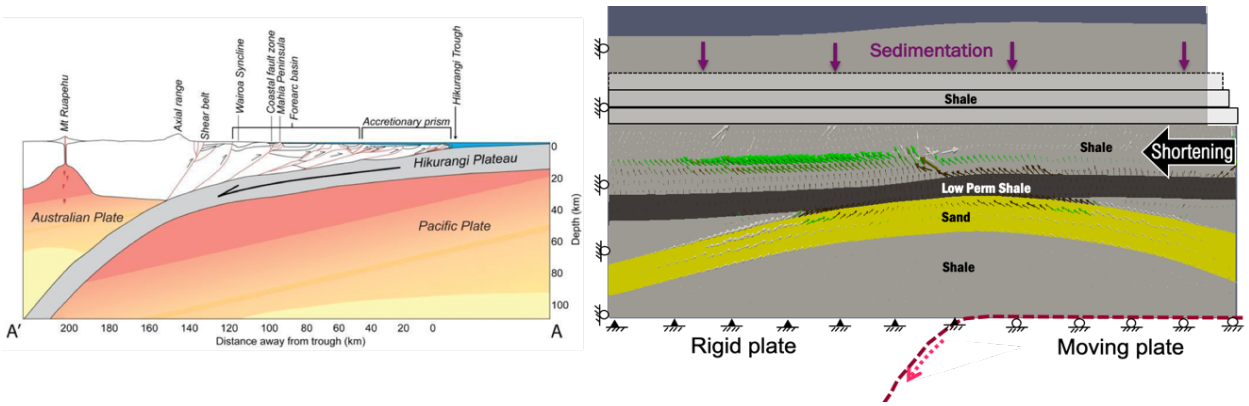

Figure 2. Comparison of complex structures overlying the Hikurangi Subduction Zone and the synthetic model where the overpressured shale system is exposed to varying degrees of horizontal shortening.

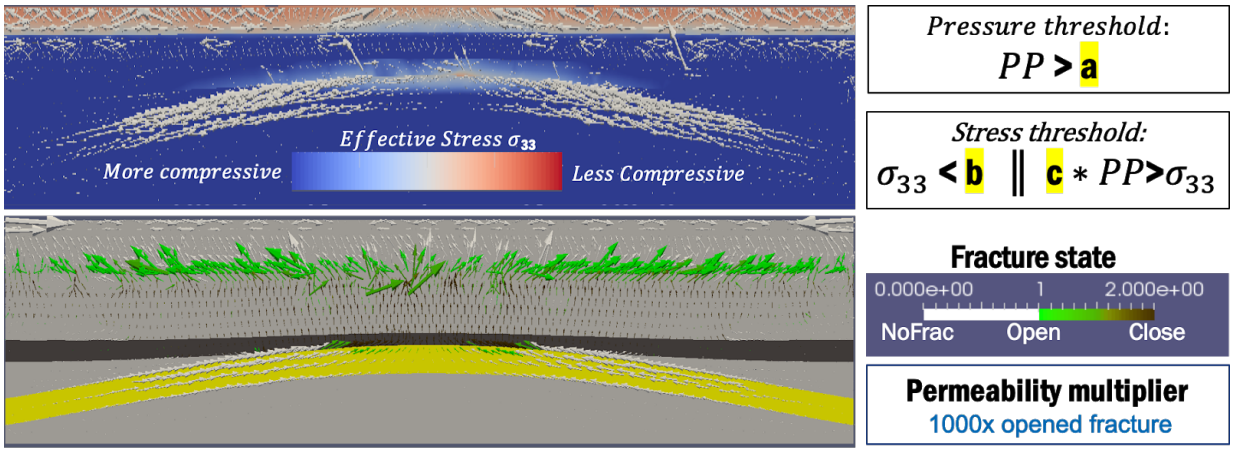

Figure 3. (A) Effective stress grid shows an area with lower compressive stress on top of the sand dome. Fracturing occurs where pore pressure and minimum effective stress meet thresholds. (B) Arrows indicate the orientation and relative magnitude of fluid flux; their colors represent fracture state at each cell. Flow from open fractures (bright green) are added by multiplied permeability during active state.

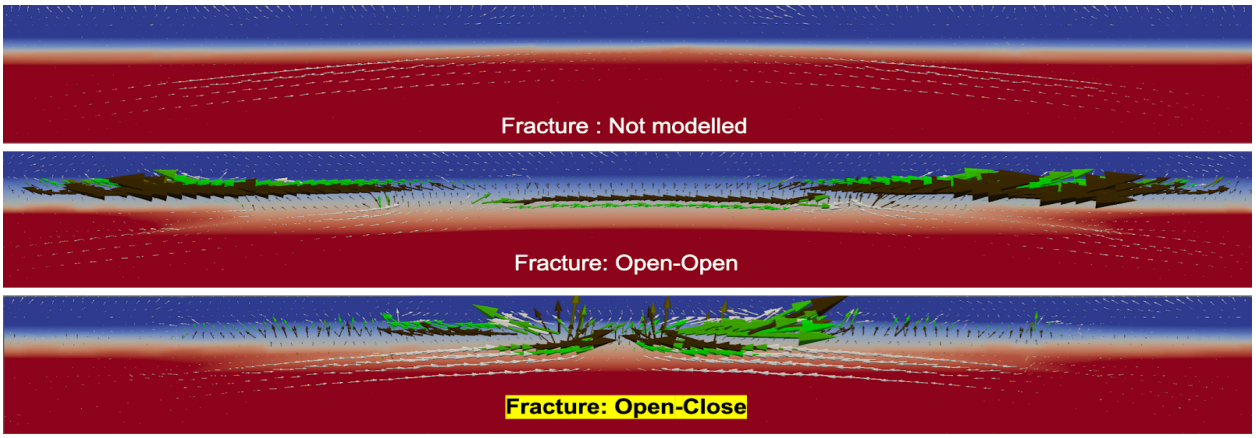

Figure 4: Overpressure plots with fluid flow overlay. Case **A** is the model that does not incorporate fracturing. Case **B** is the model where fracture remains open. Case **C** is the model that assumes dynamic fracturing as a function of pressure and stress.

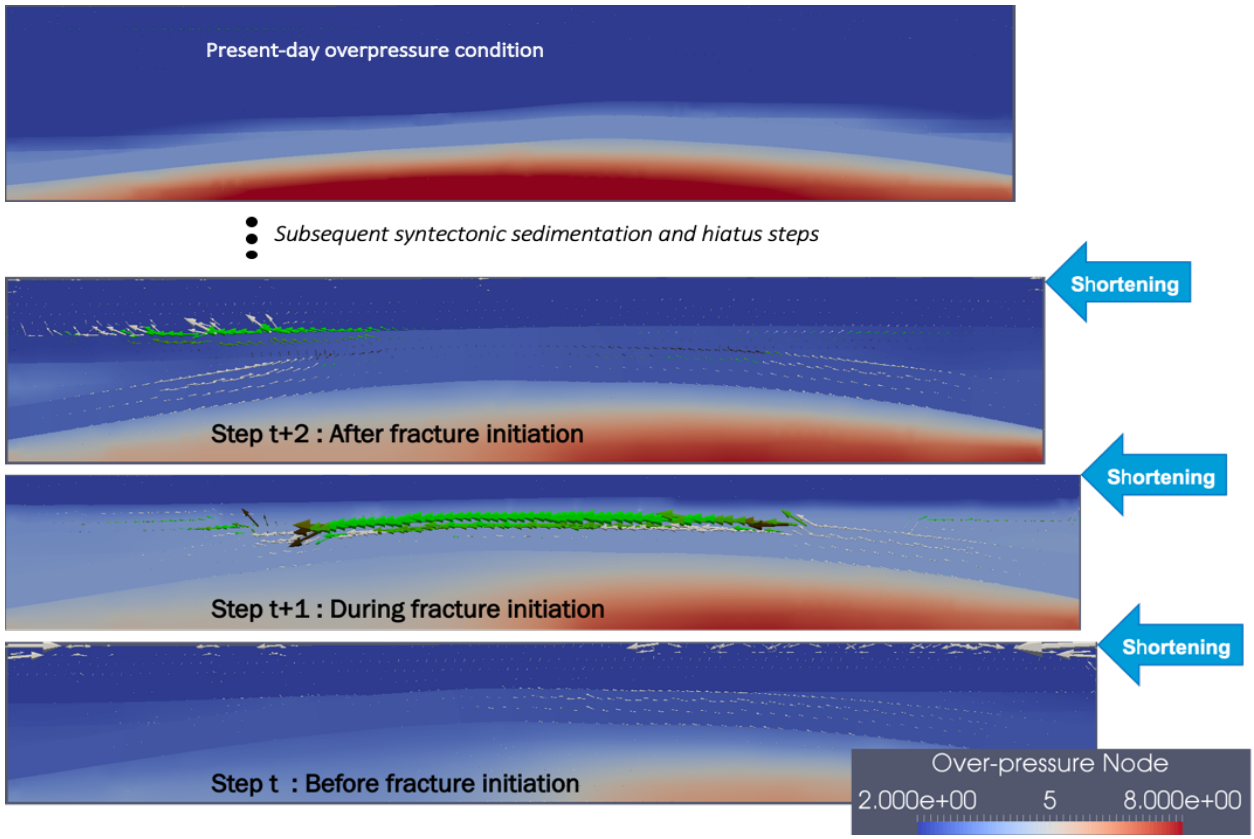

Figure 5. Evolution of pressure and fluid flow responding to dynamic fracturing and horizontal shortening: Asymmetry is observed in the model geometry, locations of fractures, and flow orientations.

References

Barnes, P. M., Lamarche, G., Bialas, J., Henrys, S., Pecher, I., Netzeband, G. L., Greinert, J., Mountjoy, J. J., Pedley, K., and Crutchley, G. [2010] Tectonic and geological framework for gas hydrates and cold seeps on the Hikurangi subduction margin, New Zealand, *Marine Geology*.

Burgreen-Chan, B., Meisling, K. E., and Graham, S. [2016] Basin and petroleum system modelling of the East Coast Basin, New Zealand: a test of overpressure scenarios in a convergent margin, *Basin Research*, **28**(4), 536–567.

Crook, A. J. L. [2013] ParaGeo: A Finite element model for coupled simulation of the evolution of geological structures, *Three Cliffs Geomechanical Analysis, Swansea, UK*.

Hantschel, T., Wygrala, B., Fuecker, M., and Neber, A. [2011] Modeling Basin-scale Geomechanics Through Geological Time, *International Petroleum Technology Conference*, (i), 6.

Neumaier, M., Littke, R., Hantschel, T., Maerten, L., Joonnekindt, J. P., and Kukla, P. [2014] Integrated charge and seal assessment in the Monagas fold and thrust belt of Venezuela, *AAPG Bulletin*.

Nicksiar, M., and Martin, C. D. [2013] Crack initiation stress in low porosity crystalline and sedimentary rocks, *Engineering Geology*, **154**, 64–76.

Obradors-Prats, J., Rouainia, M., Aplin, A. C., and Crook, A. J. L. [2016] Stress and pore pressure histories in complex tectonic settings predicted with coupled geomechanical-fluid flow models, *Marine and Petroleum Geology*.

Rutqvist, J., Wu, Y.-S., Tsang, C.-F., and Bodvarsson, G. [2002] A modeling approach for analysis of coupled multiphase fluid flow, heat transfer, and deformation in fractured porous rock, *International Journal of Rock Mechanics and Mining Sciences*, **39**(4), 429–442.

Sone, H., and Zoback, M. D. [2014] Time-dependent deformation of shale gas reservoir rocks and its long-term effect on the in situ state of stress, *International Journal of Rock Mechanics and Mining Sciences*, **69**, 120–132.

Wei, Y., and Anand, L. [2008] On micro-cracking, inelastic dilatancy, and the brittle-ductile transition in compact rocks: A micro-mechanical study, *International Journal of Solids and Structures*, **45**(10), 2785–2798.

SENSITIVITY ANALYSIS OF MIGRATION THROUGH FAULTS

Marcelo Brasil Silka[1,*]
[1]*Department of Geological Sciences, Stanford University, Stanford, CA*
[*]mbsilka@stanford.edu

Abstract

The Campos basin is one of the passive margin basins originating at the opening of the Atlantic Ocean on Brazil's shore. Layering of rock units in the Campos basin would be quite monotonous without the halokinesis of its Aptian salt layer. Together with the movement of salt, detached faults were formed. Those faults may play an important role in the transport of oil and CO_2 through the basin (Sibson, 1990, Beglinger et al., 2012). This report presents some results of the sensitivity analysis of basin properties – basically, faults on source rocks properties – on modeled values of saturation of oil and CO_2 within a volume that represents 2% of the total area of Campos basin.

A basic basin model assembled and granted by Petrobras, with 39 horizons from a northern area of Campos basin, was replicated, parametrized by 46 basin variables, and processed to produce maps of three kinds of saturations (CO_2, liquid, and vapor) at the present time. The software employed was PetroMod 3D, version 2018.1. Six of the variables are related to each of the 3 faults, the Shale Gauge Ratio (SGR), and the Fault Time Definition (FTD) that model the change during burial history of the fault's openness. The 40 other parameters are equally distributed among 5 source rock layers, namely the amount of TOC, of HI, the localization and size of an elliptic pod (5 independent variables each), and the time of deposition of the source rock (DtSR), comprised of the nominal time of the top horizon, plus a variable increment characterizing a chronostratigraphic uncertainty in exploration.

Two thousand realizations were created, and the responses were retrieved as a dataset assembled with 2000x39x3 maps (**Figure 1**). The kinetics are from Vitrimat-2018 (Burnham, 2019). The method used for Sensitivity Analysis was the Distance-based Generalized Sensitivity Analysis (DGSA) (Scheidt, Li and Caers, 2018), and it was performed using a Python code developed at the Stanford Center for Earth Resources Forecasting (SCERF, 2019).

Our ultimate interest is to study the uncertainty of migration paths using these models. The goal is to extract signatures of the movement of oil from the modeled patterns in the saturation maps. To accomplish this, several alternatives were tested to integrate the multilayer data into one single map with the quality of, firstly, indicating migration and, secondly, being capable of resolving contrasts among the diverse realizations in order to facilitate clustering of the whole set of responses.

In addition, the role of faults in the overall process was modeled by extracting projections of the resulting maps on the faults and arranging the values into arrays of data to perform DGSA. Pareto plots are presented to illustrate the findings of sensitivity so far (**Figure 2**).

Figures

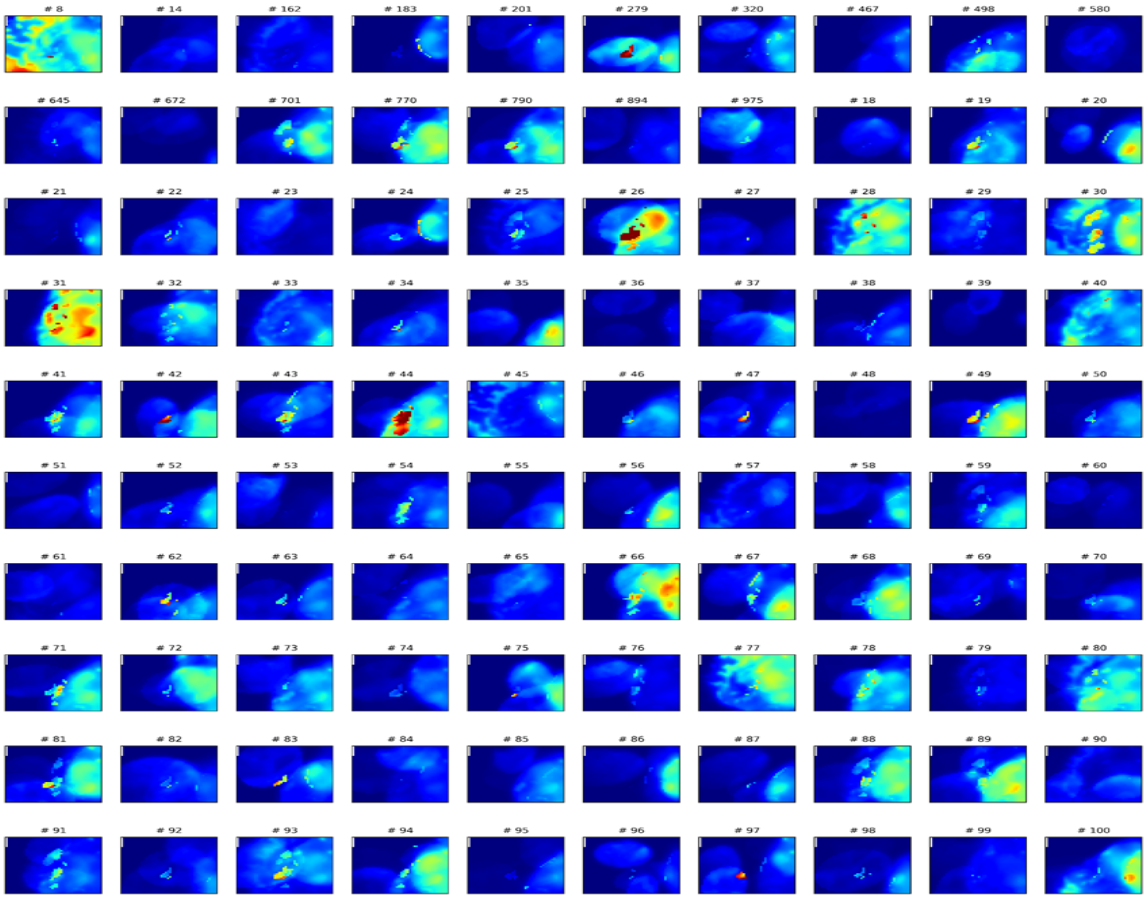

Figure 1. One hundred different realizations, from the total of 2000, of the Campos basin model depicted as maps of the mean average, vertically taken, over the 39 resulting layers of saturation of CO_2 in the present time.

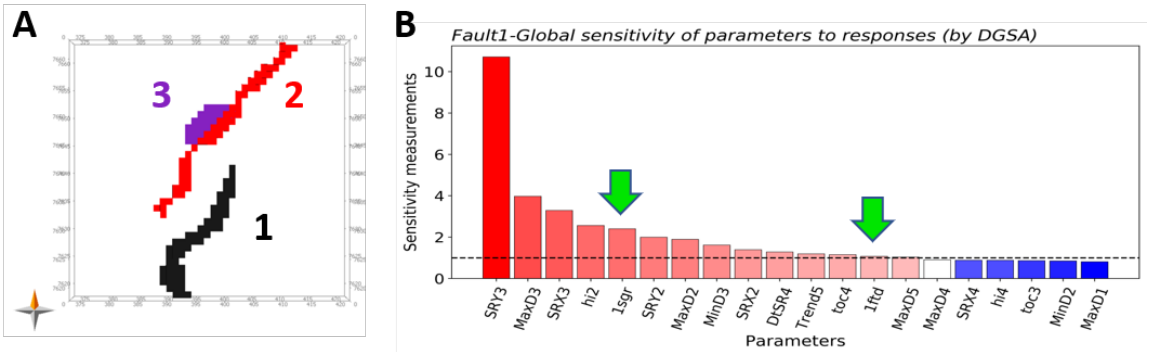

Figure 2. A) Map of localization of the faults in the model. B) Pareto plot showing the sensitivity analysis on the data of saturation of liquid projected onto Fault 1. The most

sensitive parameter is SRY3, the N-S position of Source Rock 3 (Albian). The green arrows highlight the parameters Shale Gauge Ratio (SGR) and Fault Time Dependency (FTD) related to Fault 1.

Acknowledgments

I thank Petrobras for the data and the support that allow me to pursue the doctorate at Stanford-Geological Sciences researching the uncertainty within the migration in Campos basin. I am grateful to my advisors, Jef Caers and Allegra Hosford Scheirer, for fruitful discussions and enlightening suggestions. A special recognition to Mustafa Al Ibrahim for the authorship of the MATLAB code that accelerates this research. Thank you to Schlumberger for PetroMod software.

References

Sibson, 1990: Conditions for fault-valve behavior. Deformation Mechanisms, Rheology and Tectonics, Geological Society Special Publication No. 54.

Beglinger et al., 2012: Tectonic subsidence history and source-rock maturation in the Campos Basin, Brazil. Petroleum Geoscience, Vol. 18, pp. 153 –172. DOI: 10.1144/1354-079310-049

Burnham, 2019: Kinetic models of vitrinite, kerogen, and bitumen reflectance. Organic Geochemistry, Volume 131, May 2019, Pages 50-59.

Scheidt, Li and Caers, 2018: Quantifying Uncertainty in Subsurface Systems. American Geophysical Union. DOI:10.1002/9781119325888.

SCERF, 2019: https://github.com/SCRFpublic/DGSA_Light

FAULT PROPERTIES AND RESERVOIR HETEROGENEITY IN PETROLEUM SYSTEMS MODELING RESULTS

Anatoly Aseev[1*], Allegra Hosford Scheirer[1], Tapan Mukerji[1], and Ebbe H. Hartz[2]
[1]*Department of Geological Sciences, Stanford University, Stanford, CA*
[2]*Aker BP, Oslo, Norway*
*aaseev@stanford.edu

Introduction

Basin models are used for regional estimation of hydrocarbon potential, but commonly tend to oversimplify structural and lithological architecture of the oil and gas petroleum system. This can lead to misevaluation of pore pressures, fluid volumes, seal capacity, accumulation geometry, and other important parameters during hydrocarbon prospecting.

In structurally complex targets, properties of faults play a significant role in controlling pore pressures and fluid migration over time. Lithology variation at reservoir scale adds another source of uncertainty. A common practice in basin modeling is to deterministically assign a single lithology value or a simplified map to tens or hundreds of meters of a reservoir rock layer. This approach saves computational resources, but the lack of resolution prevents robust analyses of geological information at reservoir scale.

In this study, we explore the impact of variations in fault properties and reservoir heterogeneity on 2D petroleum systems models located in the Viking Graben, North Sea.

2D petroleum systems modeling

The area of study is located in the South Viking Graben, central North Sea (**Figure** 1). The majority of the hydrocarbon traps found in the Viking Graben have an important structural component produced during phases of deformation or subsidence from Triassic to Cenozoic times. These include horst traps, footwall and hanging wall traps formed by Late Jurassic to Lower Cretaceous rifting (Ahmadi et al., 2003).

To understand the impact of reservoir rock heterogeneity on petroleum systems modeling, we converted gamma ray values from the wells in a 3D reservoir model into a corresponding set of PetroMod facies with sand-shale lithology mix. Then we performed Gaussian Sequential Simulation and simulated heterogeneous lithology in the larger scale basin model in the reservoir zone (**Figure 2**).

To understand the impact of fault properties on petroleum systems modeling, we transferred faults from a 3D reservoir model to a 3D basin model. Then we extracted a cross section and created six different models (**Table 1**), including a base case model. The base case model has no faults in the discovery area and has homogenous sand as a reservoir lithology (**Figure 3**). The rest of the 2D models have different fault properties for the same set of faults.

There are three fault properties defined in basin modeling software: shale gouge ratio (SGR), fault capillary pressure (FCP) and fault permeability (K_f). Also, a fault can be assigned as closed to flow, impermeable to flow, and open to flow. PetroMod uses an empirical equation for converting SGR to FCP (Hantschel and Kauerauf, 2009):

$$FCP = k\,(SGR - 0.18)$$

where the average value for k is 50 MPa.

According to Sperrevik et al. (2002) and Yielding et al. (2010), depth of the fault, or Z_{max} (Sperrevik et al., 2002), is one of the most important parameters controlling fault sealing. However, this variable is missing in the formula of Hantschel and Kauerauf (2009), whereas it is a standard plug-in in Petrel, and used in common workflows in oil companies. To estimate fault properties during petroleum systems evolution, we calculated FCP and K_f using Sperrevik et al. (2002) equation for every episode of deposition starting from fault initiation in the Late Jurassic. The SGR value for the modelled faults are the mean of SGR value on the fault plane taken from the 3D reservoir model.

$$k_f = a_1 exp\{-\left[a_2 SGR + a_3 z_{max} + \left(a_4 z_f - a_5\right)(1 - SGR)^7\right]\},$$

where, a_1=80000, a_2=19.4, a_3=0.00403, a_4=0.0055, a_5=12.5, z_{max} is maximum burial depth of the fault in meters and z_f is depth of faulting in meters.

$$FCP = 31.838 \cdot k_f^{-0.3848}$$

Simulation results

Simulation results demonstrated a significant difference in petroleum saturation and geometry of hydrocarbon accumulations between the base case model and models with faults and upgraded reservoir lithology (**Figure 4**). The base case model overestimates column heights, as all the hydrocarbons migrate along the reservoir layers and fill anticline traps. The geometry of the accumulation is controlled by trap closure. In contrast, migration in the faulted models are controlled by fault seal properties and capillary pressures in heterogenous reservoir rocks. Models with just open or closed faults fail to predict known oil discoveries because fluids are leak along or are stopped by fault planes bounding structural traps.

In the model with changing fault properties through time, significant leakage across fault planes occurs at the early stage of petroleum system evolution, when Zmax is low. Later, higher FCP values control influx of hydrocarbons and accumulation column height. Model with assigned FCP values through geological time show a good match between modelled and existing accumulations. Thus, in structurally complex areas, such as the Viking Graben, faults and their properties likely play an important role in oil and gas prospecting. Careful estimation of SGR and FCP values of the faults in 2D basin modeling can decrease exploration risks associated with migration, charge, and accumulation geometry.

Figures

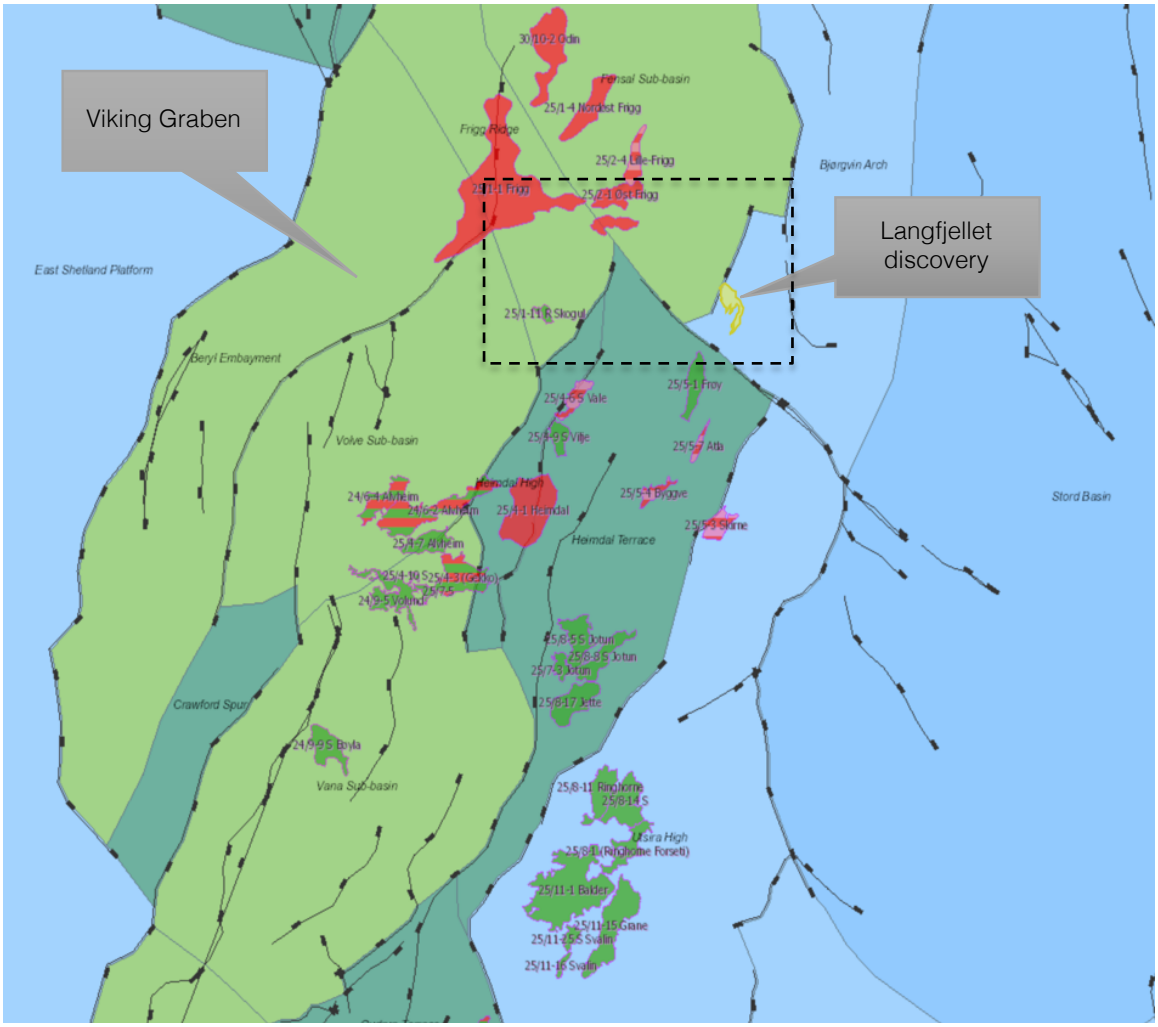

Figure 1. Location of area of interest

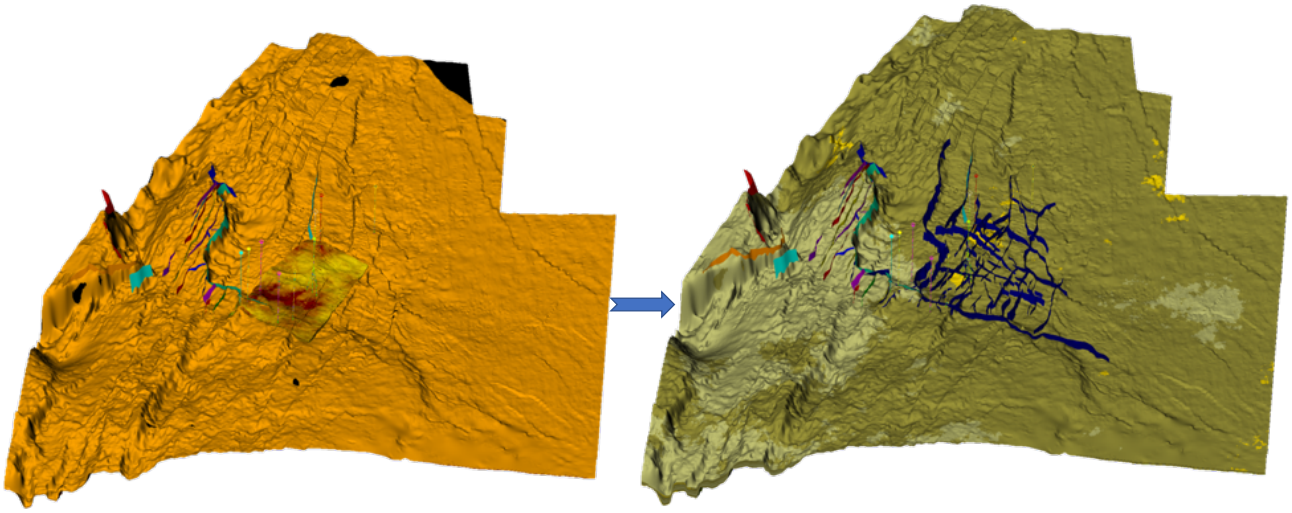

Figure 2. Facies distribution from local 3D reservoir model (small inset area in the middle of the map, left) onto basin model (large map area, right)

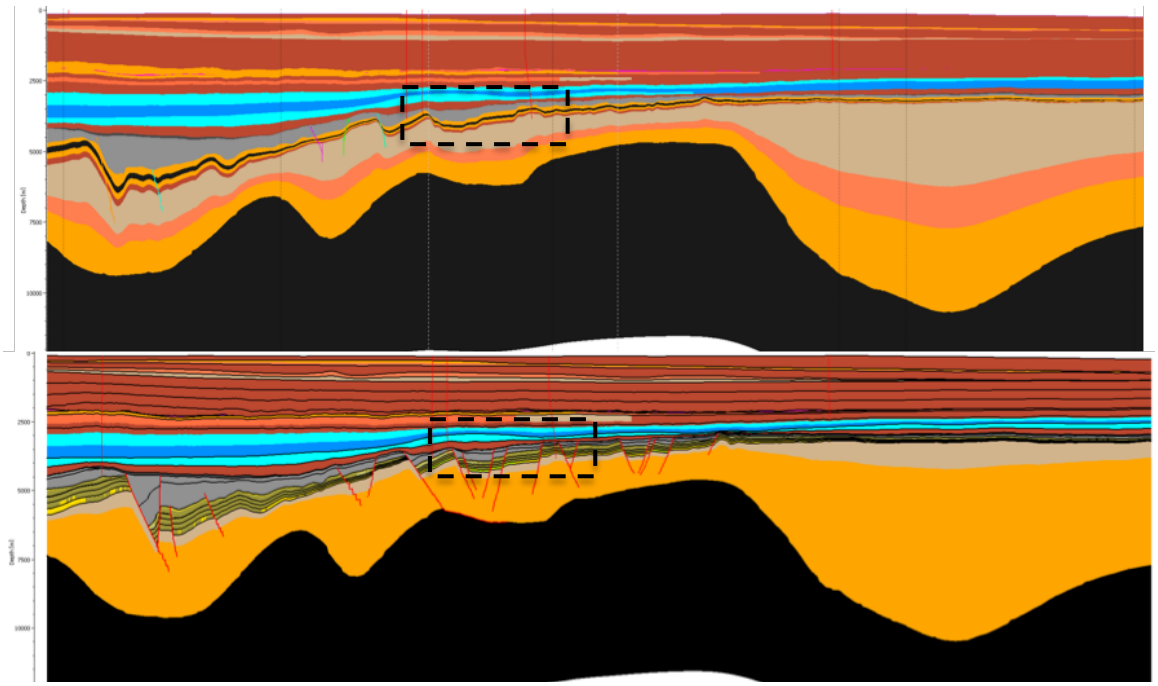

Figure 3. Base case model with no faults in oil discovery area (top) and upgraded model (bottom). Black rectangle shows the area of oil discovery.

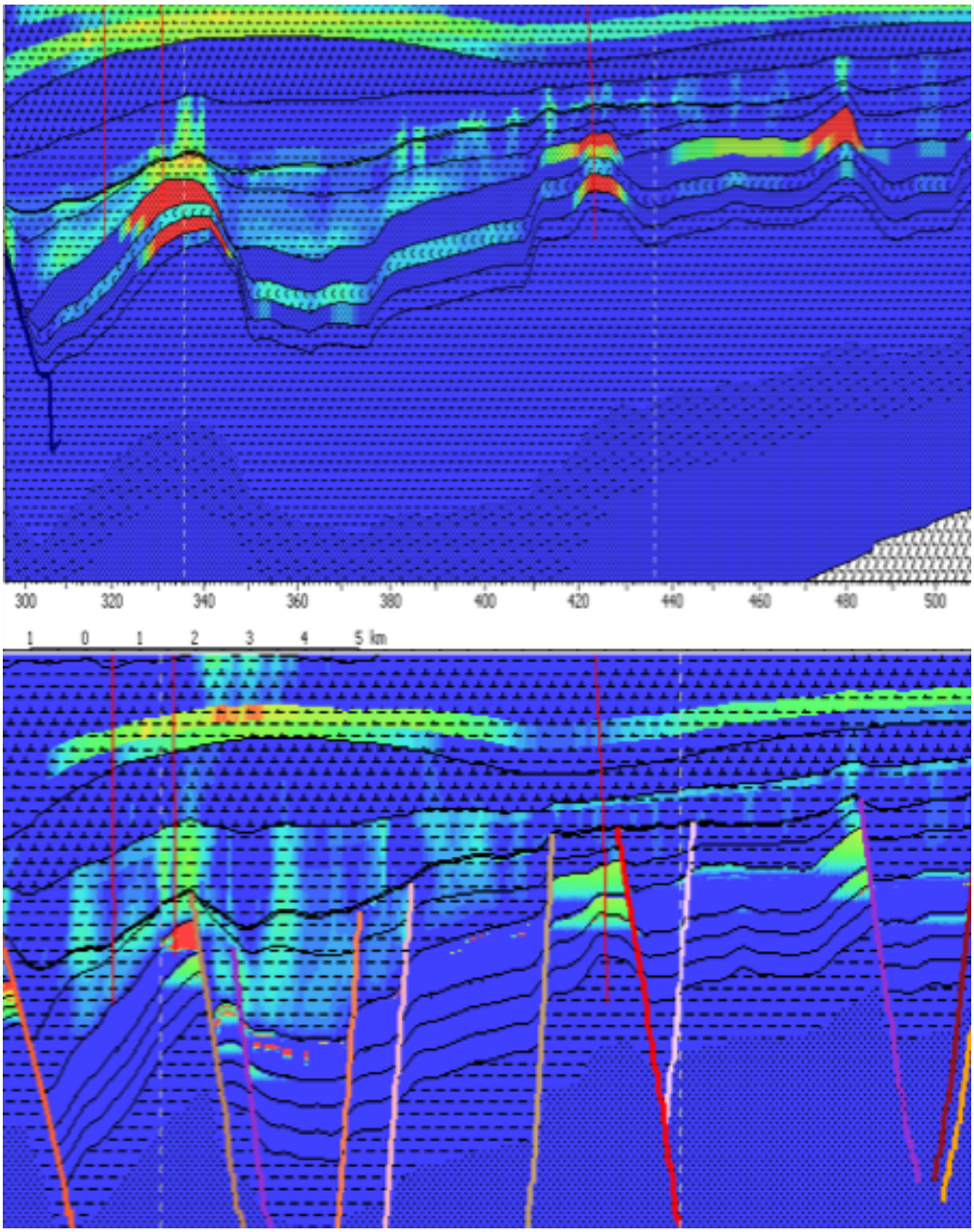

Figure 4. Significant difference in petroleum saturation between base case model (top) and one of the models with upgraded facies and faults (bottom)

Table 1. Simulated 2D models and their reservoir heterogeneity and assigned fault properties

Model name	**Reservoir heterogeneity**	**Fault Properties**
Base case	Homogenous Sand	Open/Closed
Petromod_FCP/Kf_LGR	Heterogenous sand-shale	FCP using Hantschel and Kauerauf formula
Sperrevik_FCP/Kf_LGR	Heterogenous sand-shale	FCP using Sperrevik formula
Open_LGR	Heterogenous sand-shale	Open
Closed_LGR	Heterogenous sand-shale	Closed
Sperrevik_FCP/Kf_LGR_19episodes	Heterogenous sand-shale	FCP using Sperrevik formula for nineteen episodes of deposition

Acknowledgments

We would like to thank Aker BP for providing geological data for this ongoing research. Thank you to Schlumberger for PetroMod software.

References

Ahmadi, Z., M. Sawyers, S. E. M. G. Kenyon-Roberts, D. Paleocene. In: Evans, K. K.A, J. Fugelli, and P. (eds) 235-259 G. C. A. A. Bathurst, 2003, The Millenium Atlas: Petroleum geology of the central and northern North sea: doi:DOI: 10.1017/S0016756803218124.

Hantschel, T., and A. I. Kauerauf, 2009, Fundamentals of basin and petroleum systems modeling: doi:10.1007/978-3-540-72318-9.

Sperrevik, S., P. A. Gillespie, Q. J. Fisher, T. Halvorsen, and R. J. Knipe, 2002, Empirical estimation of fault rock properties: Norwegian Petroleum Society Special Publications, doi:10.1016/S0928-8937(02)80010-8.

Yielding, G., P. Bretan, and B. Freeman, 2010, Fault seal calibration: a brief review: Geological Society, London, Special Publications, doi:10.1144/SP347.14.

REDUCING UNCERTAINTY USING WELL DATA IN 3D MODEL OF THE JEANNE D'ARC BASIN

Tanvi Chheda[1], Tapan Mukerji[2], Allegra Hosford Scheirer[1], Stephan Graham[1], and Jef Caers[1]

[1]*Department of Geological Sciences, Stanford University, CA*

[2]*Department of Energy Resources Engineering, Stanford University, CA*

[*]tanvic@stanford.edu

Introduction

In basin and petroleum system modeling, because of the large number of input parameters and insufficient and imperfect data, uncertainty exists in modeling results. It is important to characterize this uncertainty and communicate predictions in a probabilistic manner. We propose a structured workflow to calibrate models to observed data and incorporate newly available data without the need to rerun basin models. Automating both the calibration and simulation steps in basin modeling greatly reduces the need for continuous human interaction so that models honor observed data more quickly, more robustly, and less subjectively. We demonstrate this new workflow for uncertainty reduction in 3D models created from data in the Jeanne d'Arc basin in the prolific Grand Banks region offshore Newfoundland, Canada.

The main source rock in the basin, the Egret Member of the Ranking Formation, was deposited in the Late Jurassic. This was followed by rifting due to the opening of the North Atlantic in the Early Cretaceous, and episodic uplift and erosion that deposited many reservoir rock intervals until the Late Cretaceous. Albian-Aptian rifting from Greenland created major structural traps, and thick overburden was deposited in the Cenozoic (Grant and McAlpine, 1990; Richards *et al.*, 2010; Sinclair, 1993). Although this is the broadly accepted geologic history, studies differ in the details. These different hypotheses are considered to create multiple basin models with varying thermal histories, fault permeabilities, and facies distribution.

Methods

Baur *et al*. (2010) find that there was no significant increase in heat flow associated with the Albian-Aptian rifting event, whereas other authors assume otherwise. We created 120 different heat flow histories by sampling Gaussian distributions in two dimensions: age and intensity of heat flow (**Figure 1**). Both age and heat flow influence predicted temperature and vitrinite reflectance. At the same time, we vary the slope of the porosity-permeability curve and the capillary entry pressure of important horizons (**Figure 2**), as these properties can be assumed to be independent of basal heat flow in this basin. Finally, we consider different facies maps for the Egret source rock. We added faults to the model using discontinuities in the geologic horizons (**Figure 3**), and assigned times when the faults were active according to their orientation. The uncertainty lies in scenarios for when

faults are open and closed. Variable timing and extent of closure will be considered in upcoming work.

These 120 3D basin models took about 350 hours to run. Simulation results were extracted using a workflow of MATLAB for changing inputs, Schlumberger's Open Simulator for exporting output at every cell in the model, and Python programming for finding the set of cells that correspond to well locations.

Using measured data from the openly accessible BASIN database from Natural Resources Canada, we calculated summary statistics for pressure, temperature, and vitrinite reflectance. After applying quality control rules to the data, 23 wells had some reliable data. We used these in a Bayesian Network along with predictions of these quantities from the models to select the subset of models that honored the data.

Results

Models with moderately high heat flows in both rifting events best matched temperature data. West-northwest faults of age between 150 and 120 million years played a key role in the observed pressures and accumulations. Faults along trans-basinal fault trend, and in orientation close to basin bounding faults, are closed in all valid models. In most wells, the models fail to simulate high pressure at depth (**Figure** 4). This is true for both the Hibernia and Jeanne d'Arc reservoirs.

Discussion and Conclusion

The parameter space of properties of seal rocks corresponding to Hibernia and Jeanne d'Arc reservoir rocks is probably too sparse, thus more models need to be run with higher sealing capacities. The kinetics of source rock facies need to be further explored to explain the high gas-to-oil ratio in the northeastern part of the basin. In the next year, this work will be extended to codify structured decision making that is informed by a quantitative evaluation of risks and returns from exploration decisions. Although shown with the example of a conventional offshore basin in the east coast of Canada, this is fundamentally applicable to various basin types, locations, and decisions scenarios.

Figures

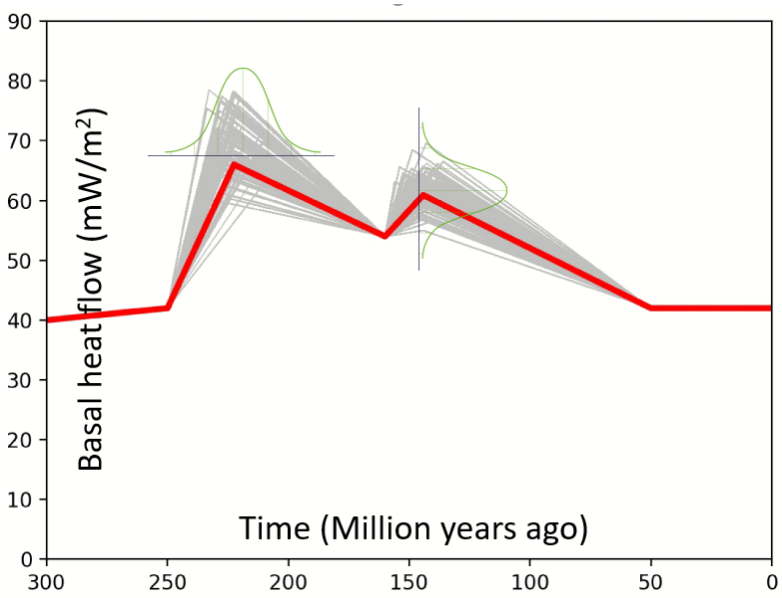

Figure 1. Basal heat flow scenarios due to uncertainty in contribution from different rifting phases.

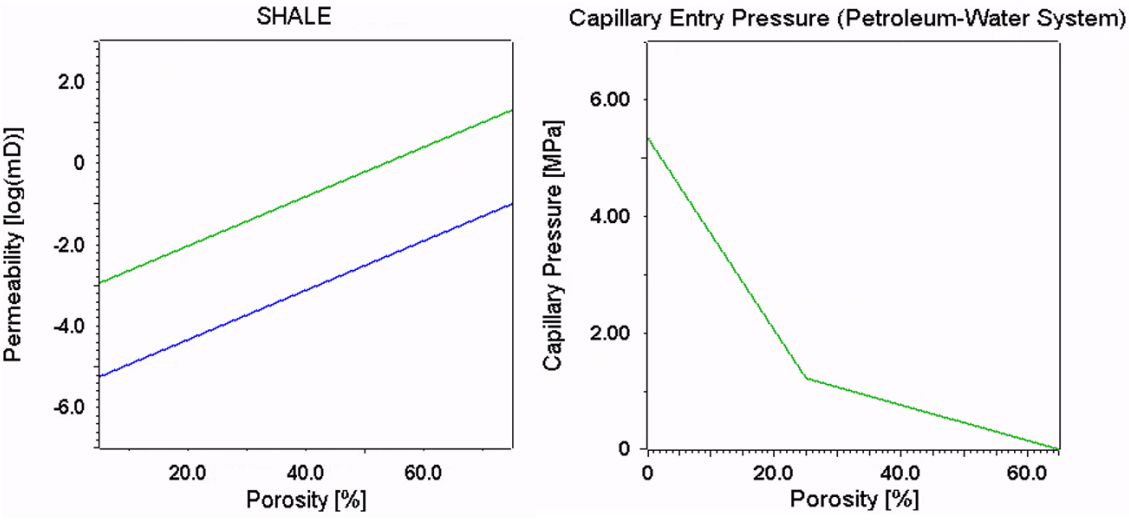

Figure 2. Base case scenario for porosity-permeability and porosity-capillary entry pressure relationship for shale. Normal distributions were sampled around the slope and intercept to obtain other scenarios.

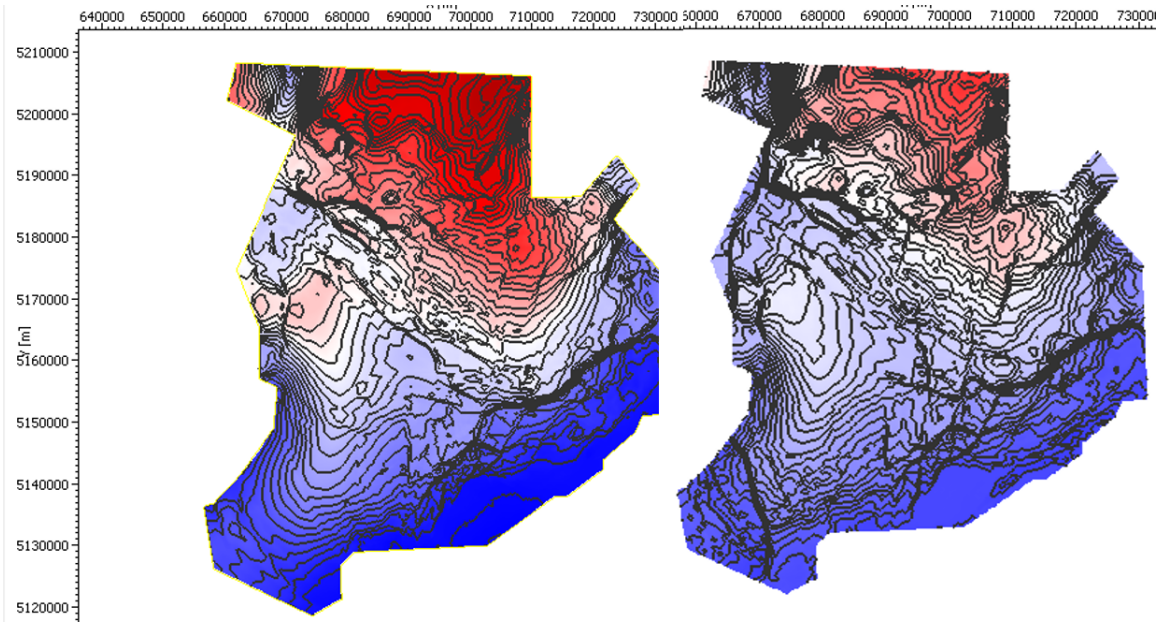

Figure 3. Horizon maps enhanced to interpret faults.

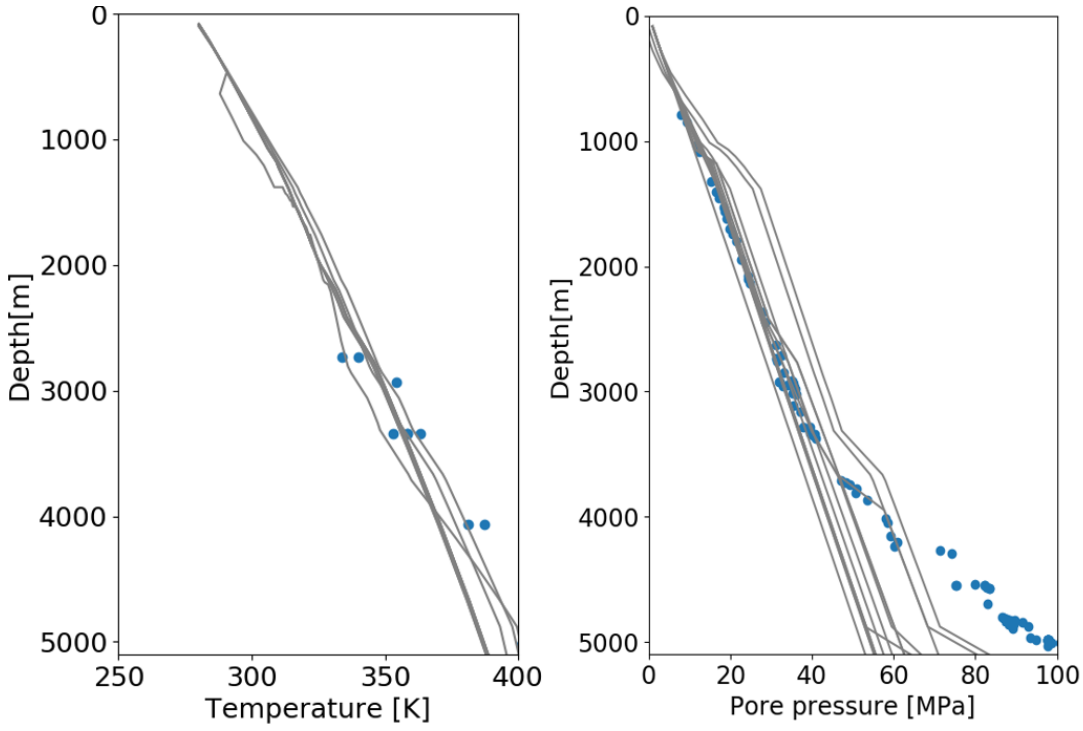

Figure 4. An example of model output and data in the South Mara I-13 well.

References

Baur, F. *et al.* (2010) 'Basin modeling meets rift analysis - A numerical modeling study from the Jeanne d'Arc basin, offshore Newfoundland, Canada', *Marine and Petroleum Geology*, 27(3), pp. 585–599. doi: 10.1016/j.marpetgeo.2009.06.003.

Grant, A. C. and McAlpine, K. D. (1990) 'The Continental Margin around Newfoundland', in *Geology of the Continental Margin of Eastern Canada*, pp. 241–292. doi: 10.4095/132690.

Sinclair, I. K. (1993) 'Tectonism: the dominant factor in mid-Cretaceous deposition in the Jeanne d'Arc Basin, Grand Banks', *Marine and Petroleum Geology*, 10(6), pp. 530–549. doi: 10.1016/0264-8172(93)90058-Z.

QUANTITATIVE SEISMIC INTERPRETATION IN ORGANIC-RICH MUDROCKS: SHUBLIK FORMATION, NORTH SLOPE, ALASKA

Mustafa Al Ibrahim* and Tapan Mukerji
Department of Energy Resources Engineering, Stanford University, CA
*Now at: Saudi Aramco, mustafa.geoscientist@outlook.com

Abstract

Estimating the lateral heterogeneity of geochemical properties of organic rich mudrocks is important for unconventional resource plays. Mature regions can rely on abundant well data to build empirical relationships and on traditional geostatistical methods to estimate properties between wells. However, well penetration in emerging plays are sparse and so these methods will not yield good results. In this case, quantitative seismic interpretation (QSI) might be helpful in estimating the desired properties. In this study, we use QSI based on rock physics template in estimating the uncertainty of the geochemical properties of organic mudrocks of the Shublik Formation, North Slope, Alaska. A rock physics template incorporating lithology, pore fraction, kerogen fraction, and maturation is constructed and validated using well data. The template clearly shows that the inversion problem is non-unique. Inverted impedances cubes are estimated from three seismic angle gathers (near with angles between 0° and 15°, mid with angle gather between 15° and 30°, and far with angle gathers between 30° and 45°). The inversion is done using a model-based implementation with an initial earth model derived from the seismic velocity model used in the processing phase. By combining the rock physics template and the results of seismic inversion, multiple realizations of total organic content (TOC), matrix porosity, and brittleness index are generated. These parameters can be used for sweet spot detection. Lithological results can also be used as an input for basin and petroleum system modeling.

INVENTORY OF ORGANIC PROPERTIES OF SHALLOW SEDIMENTS WITH APPLICATION TO BASIN MODELING OF GAS HYDRATE SYSTEMS

Zachary F. M. Burton[1,*], Laura N. Dafov[1], Allegra Hosford Scheirer[1]
[1]*Department of Geological Sciences, Stanford University, Stanford, CA*
[*]zburton@stanford.edu

Abstract

Global marine gas hydrate accumulations rival in size all known organic carbon sources, and represent a significant potential energy resource (Kvenvolden, 1995; Collett et al., 2015). Biogenic gas accumulations represent more than one-fifth of global gas resources (Rice and Claypool, 1981; Katz, 2011). Understanding the formation of these accumulations and understanding the volumes of gas resources produced and accumulated is limited, yet is critical to accurate quantitative assessment of potentially economic accumulations. Promisingly, recent advances in basin and petroleum system modeling (BPSM) provide opportunity for successful and insightful assessment of biogenic gas and particularly gas hydrate systems.

Here we compile a global database of sediment organic properties critical to the modeling of gas and gas hydrate volumetrics. We gather total organic carbon (TOC) and hydrogen index (HI) measurements from global drilling data at 43 known marine gas hydrate sites (**Figure 1**), and also compile properties used in six recent BPSM studies of gas hydrate (**Figure 2**). Across five continents (North America, South America, Europe, Asia, and Australia) where gas hydrate locality sediment organic properties are available, we find average TOC is ~1.2% (median 1.1%) and minimum TOC is 0.3% (**Figures 3 and 4**), while average HI is ~170 (median 150) and minimum HI is 50 (**Figures 5 and 6**). We conclude that average gas hydrate-associated TOC values of 0.3 to over 3% are compatible with previous studies suggesting a minimum TOC of 0.4 to 0.5% needed for gas hydrate formation (Waseda, 1998; Klauda and Sandler, 2005), and that HI values associated with sites of recovered or inferred gas hydrate ranging from 25 to over 400, as well as previous BPSM modeling results (Fujii et al., 2016), generally suggest that an HI as low as 50 to 60 can result in gas hydrate formation. Our compilation provides global sediment organic properties that may be utilized in any future BPSM study of biogenic gas and particularly gas hydrate systems, and also provides further understanding of minimum thresholds of TOC and HI necessary for the formation of gas hydrate.

As a complement to our global inventory, we construct a 3-D synthetic BPSM model (**Figures 7 and 8**) to simulate gas hydrate formation under favorable geologic conditions (i.e., via both structural and stratigraphic focusing of gas migration) and with varying input values for TOC and HI. This allows us to query and quantitatively investigate the minimum sediment organic property values needed for gas hydrate formation. We find that two strikingly low sediment organic property scenarios – Scenario 1 with 0.1% TOC and 100 HI, and Scenario 2 with 0.2% TOC and 50 HI – are able to produce some amount of gas hydrate saturation at the crest of a four-way closure (dome) with a connected "open" fault (**Figures**

9 and 10). Scenario 1 is consistent with previous work on minimum TOC values needed for microbial gas generation, which demonstrated that a free gas phase can be produced with a TOC as low as 0.12% under hydrostatic pressures (Clayton, 1992). Scenario 2 is consistent with both the results of our global organic properties compilation and with previous modeling work (Fujii et al., 2016), which suggest that an HI as low as 50 or 60 may allow for accumulation of gas hydrate.

Taken together, our global compilation and our synthetic modeling efforts are consistent with general minimum sediment organic property values of 0.4 to 0.5% TOC and 50 to 60 HI, but also suggest that under highly favorable geologic conditions (i.e., structural and stratigraphic focusing), a TOC as low as 0.1% or HI as low as 50 may produce sufficient free gas to allow for gas migration and accumulation in the form of gas hydrate. With global TOC for even sandy sediments ranging from 0.2% and up (Waksman, 1933), our results perhaps indicate that, under favorable geologic conditions, sediment organic properties may not represent a limiting factor in the formation of gas hydrate.

Figures

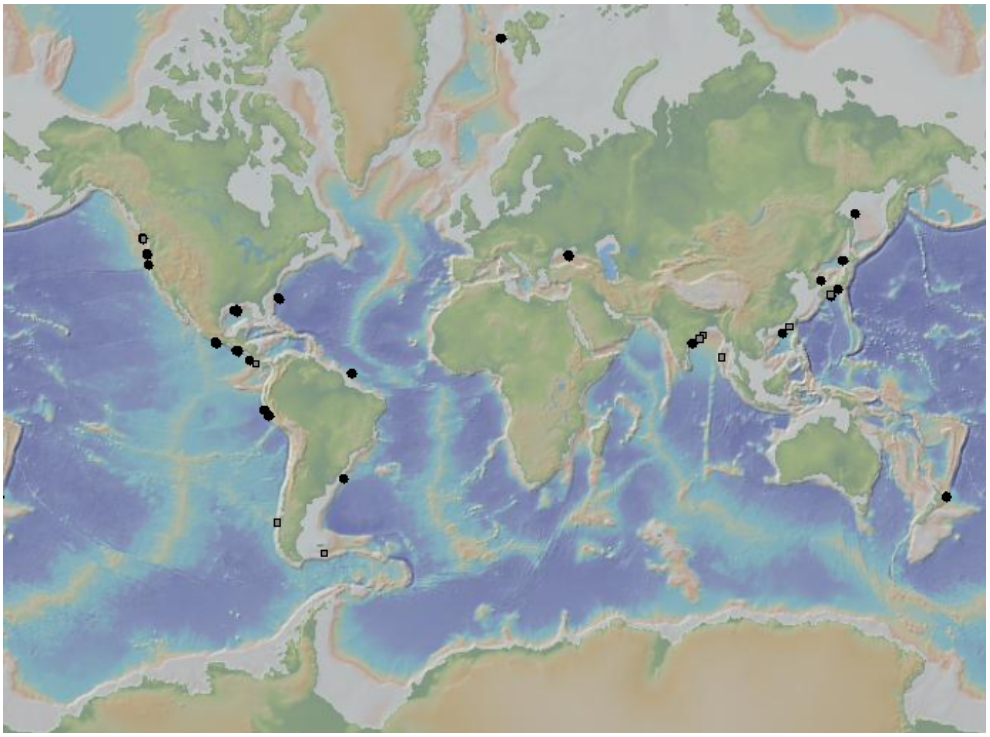

Figure 1. Drilling sites from which TOC and HI data were compiled. Black circles are sites from which gas hydrate was successfully recovered whereas gray square indicates locations where presence of gas hydrate is inferred. Base map from GeoMapApp, 2019.

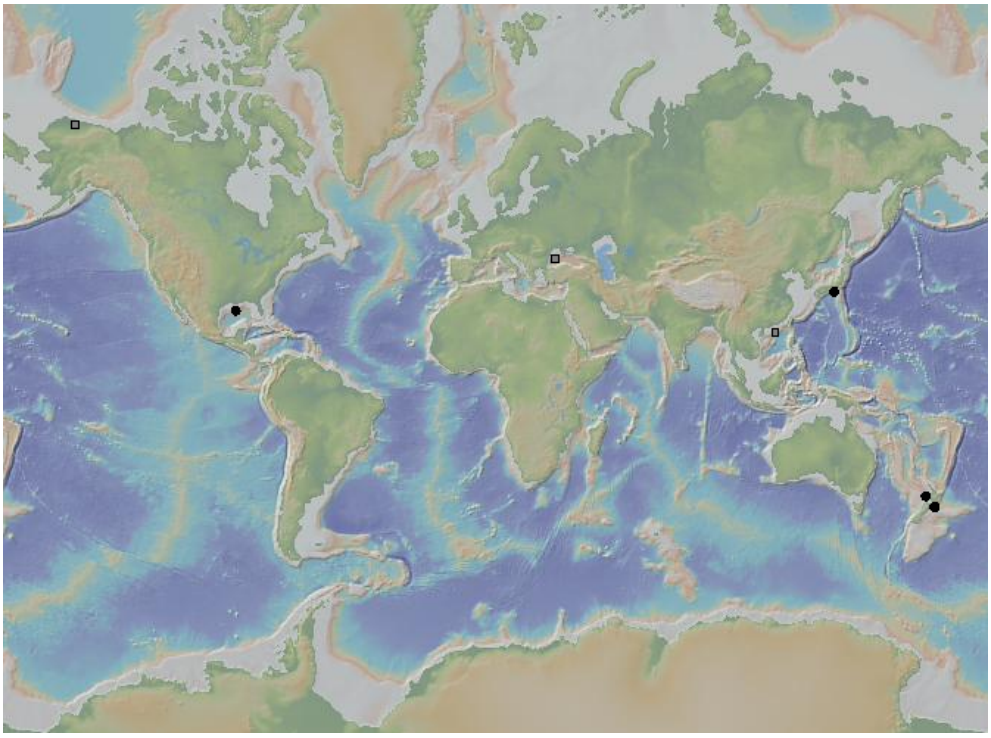

Figure 2. Geographic location of existing BPSM studies published to date. Black circles are studies with published TOC and HI values whereas gray squares are studies that did not use or did not publish TOC and HI values. Base map from GeoMapApp, 2019.

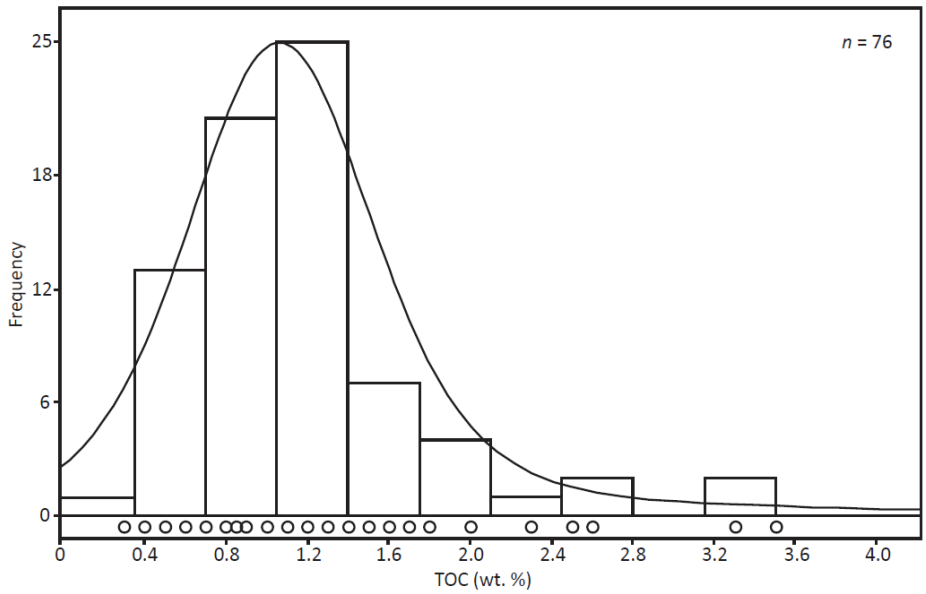

Figure 3. Kernel density estimation function (solid line) and histogram (rectangles) describing the distribution of published TOC values associated with sites where gas hydrate has been recovered.

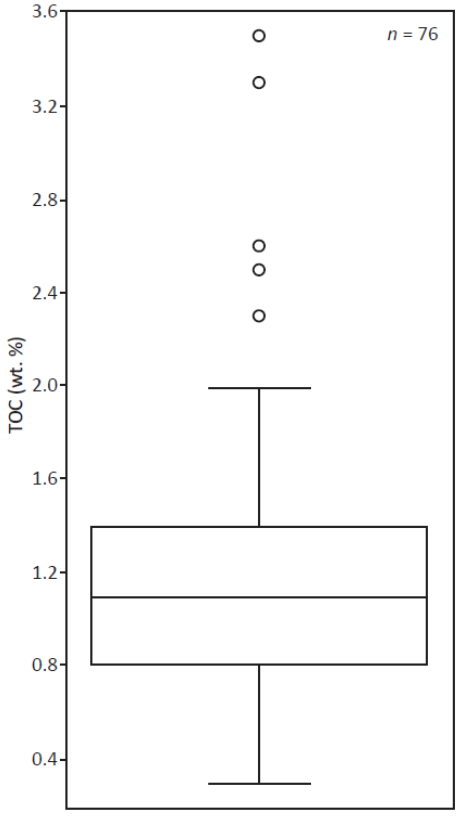

Figure 4. Box plot for published TOC values associated with sites where gas hydrate has been recovered. Average TOC is ~1.2±0.6 wt. %, median is 1.1 wt. %. Minimum TOC is 0.3 wt. %, maximum TOC is 3.5 wt. %, first quartile is ~0.8 wt. %, and third quartile is 1.4 wt. %.

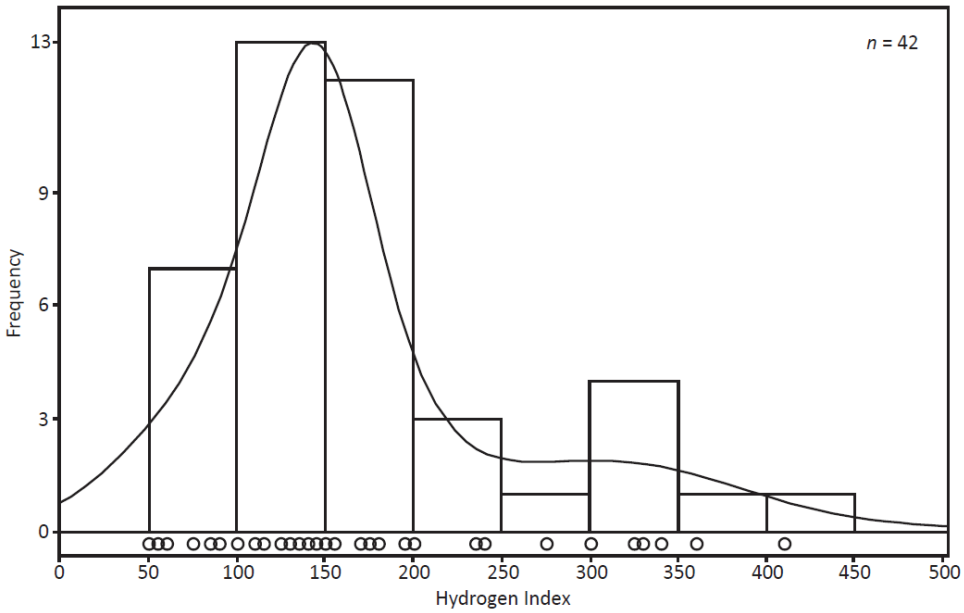

Figure 5. Kernel density estimation function (solid line) and histogram (rectangles) describing the distribution of published HI values associated with sites where gas hydrate has been recovered.

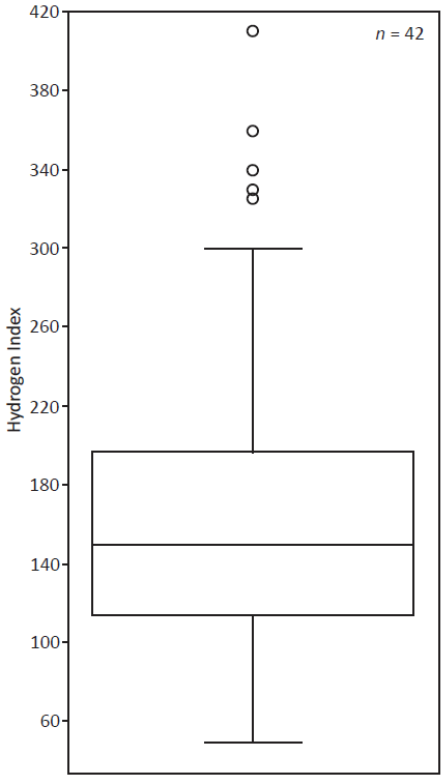

Figure 4. Figure 6. Box plot for published HI values associated with sites where gas hydrate has been recovered. Average HI is ~170±85 mg HC/g TOC, median is 150 mg HC/g TOC. Minimum HI is 50 mg HC/g TOC, maximum is 410 mg HC/g TOC, first quartile is ~115 mg HC/g TOC, and third quartile is ~195 mg HC/g TOC.

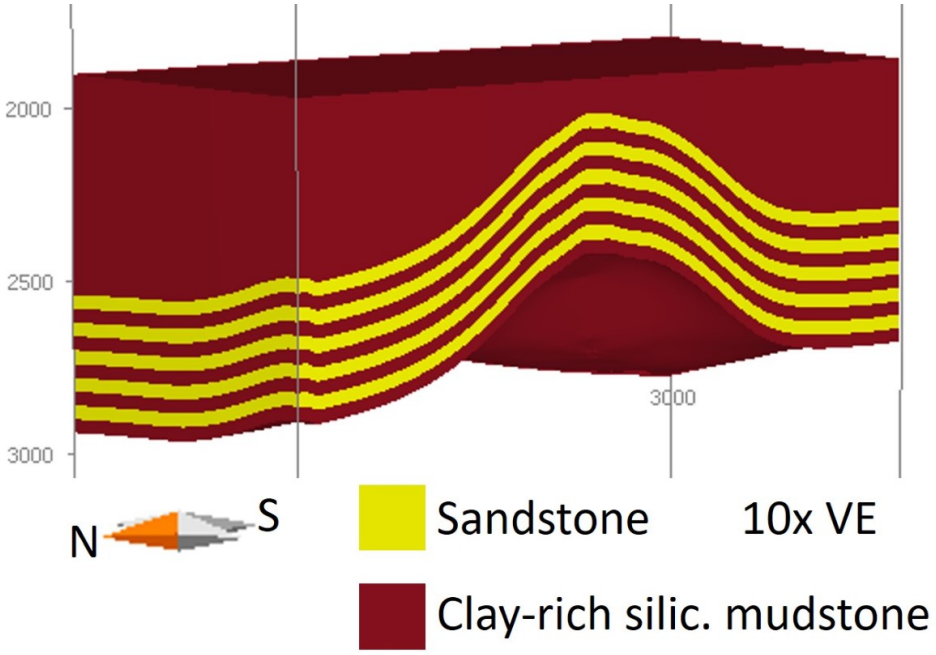

Figure 7. 3-D synthetic model simulating a four-way closure (anticline) with intercalated sand and shale lithologies. Depth in m.

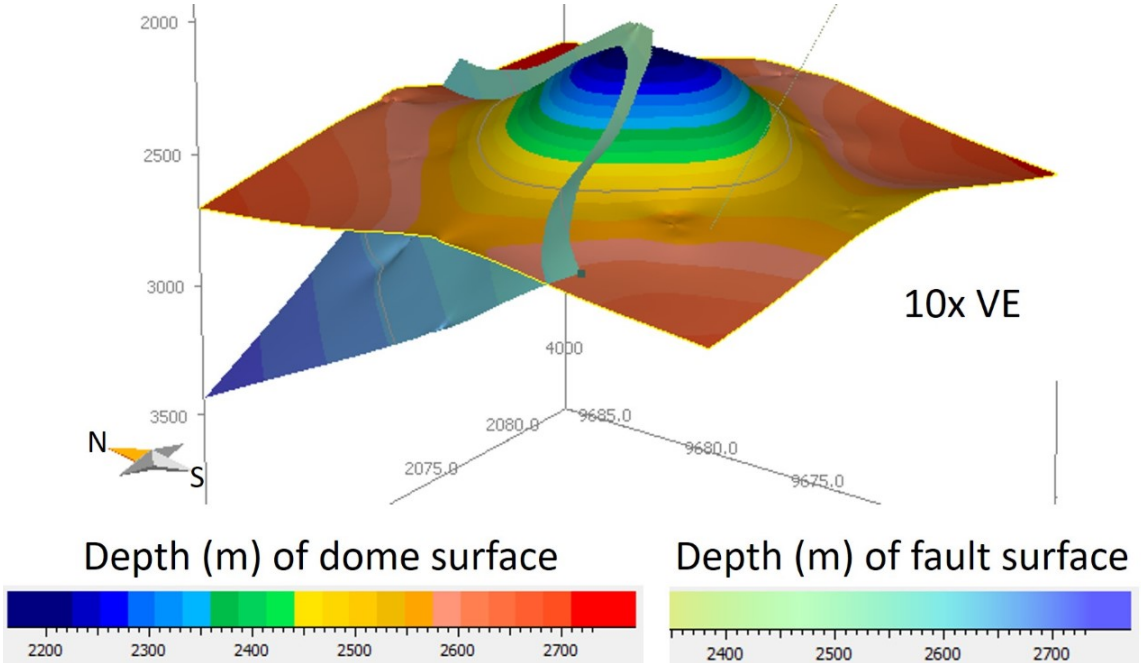

Figure 8. 3-D synthetic model simulating a four-way closure (anticline) with a through-cutting open fault.

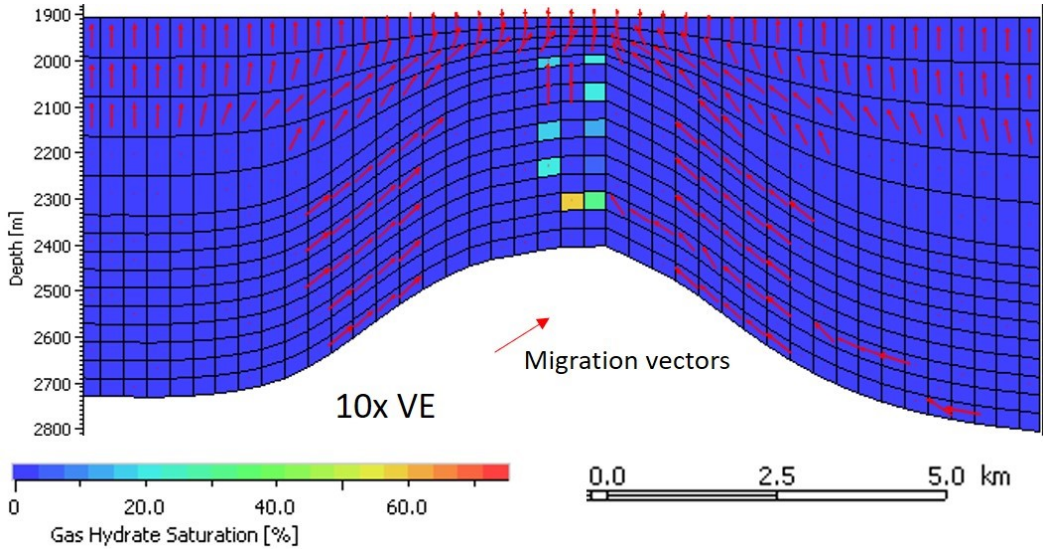

Figure 9. Cross section of simulated 3-D model highlighting elevated (>50%) gas hydrate saturations at the crest of folded lithologies within the anticline. Results shown for Scenario 1 (0.1% TOC and 100 HI (mg HC/g TOC).

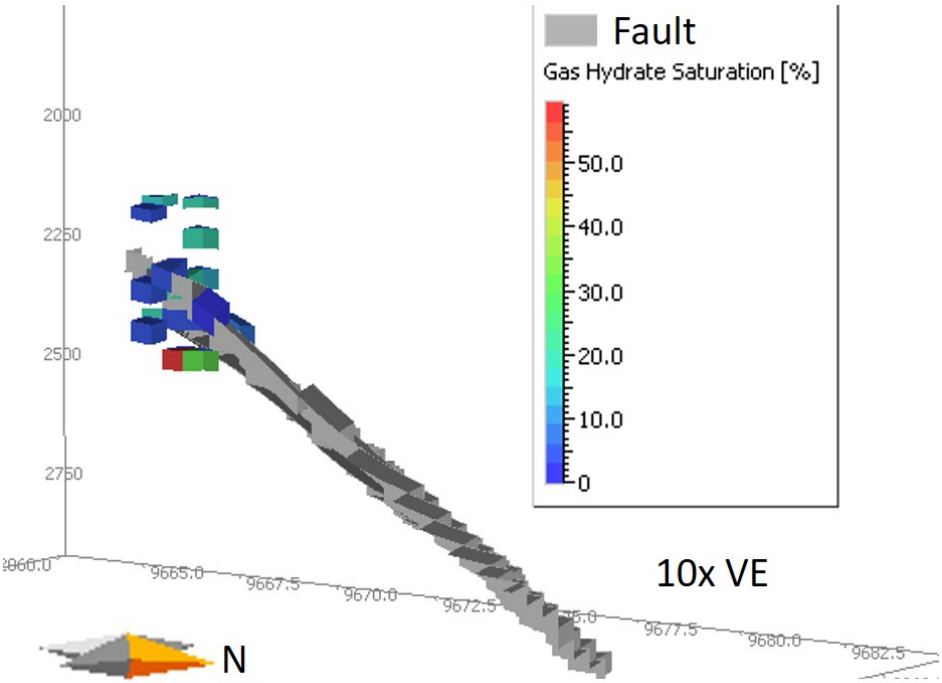

Figure 10. Visualization of open fault (grey) and cells with >0% gas hydrate saturations. Results shown for Scenario 1 (0.1% TOC and 100 HI). Depth in m.

Acknowledgments

Funding to Z.F.M.B. for gas hydrate system work was provided by the Stanford University Basin and Petroleum System Modeling (BPSM) Industrial Affiliates Group, the U.S. Department of Energy National Energy Technology Laboratory (NETL), the AAPG Grants-in-Aid Program, and the Stanford McGee/Levorsen fund. We thank Anatoly Aseev and Yongkoo Seol for assistance and input. Thank you to Schlumberger for PetroMod software.

References

Clayton, C. "Source volumetrics of biogenic gas generation." In R. Vially, ed., Bacterial Gas: pp. 191-204. Editions Technip, Paris, 1992.

Collett, Tim, Jang-Jun Bahk, Rick Baker, Ray Boswell, David Divins, Matt Frye, Dave Goldberg et al. "Methane Hydrates in Nature–Current Knowledge and Challenges." *Journal of Chemical & Engineering Data* 60, no. 2 (2015): 319-329.

Fujii, Tetsuya, Than Tin Aung, Naoya Wada, Yuhei Komatsu, Kiyofumi Suzuki, Toshiyasu Ukita, Bjorn Wygrala, Thomas Fuchs, Wolf Rottke, and Kosuke Egawa. "Modeling gas hydrate petroleum systems of the Pleistocene turbiditic sedimentary sequences of the Daini-Atsumi area, eastern Nankai Trough, Japan." *Interpretation* 4, no. 1 (2016): SA95-SA111.

Katz, Barry Jay. "Microbial processes and natural gas accumulations." *The Open Geology Journal* 5, no. 75 (2011): 75-83.

Klauda, Jeffery B., and Stanley I. Sandler. "Global distribution of methane hydrate in ocean sediment." *Energy & Fuels* 19, no. 2 (2005): 459-470.

Kvenvolden, Keith A. "A review of the geochemistry of methane in natural gas hydrate." *Organic Geochemistry* 23, no. 11-12 (1995): 997-1008.

Rice, Dudley D., and George E. Claypool. "Generation, accumulation, and resource potential of biogenic gas." *AAPG Bulletin* 65, no. 1 (1981): 5-25.

Waksman, Selman A. "On the distribution of organic matter in the sea bottom and the chemical nature and origin of marine humus." *Soil Science* 36, no. 2 (1933): 125-147.

Waseda, Amane. "Organic carbon content, bacterial methanogenesis, and accumulation processes of gas hydrates in marine sediments." *Geochemical Journal* 32, no. 3 (1998): 143-157.

THREE-DIMENSIONAL BASIN MODEL OF TERREBONNE BASIN, GULF OF MEXICO GAS HYDRATE SYSTEM

Laura Dafov[1,*], Allegra Hosford Scheirer[1], Zachary Burton[1], Nicole Masurek[2], Seth Haines[3], and Stephan Graham[1]

[1]Department of Geological Sciences, Stanford University, Stanford, California, USA
[2]Schlumberger Center of Excellence for Petroleum Systems Modeling, Aachen, Germany
[3]US Geological Survey, Boulder, Colorado, USA
[*]ldafov@stanford.edu

Abstract

Basin and petroleum system modeling (BPSM) is a dynamic quantitative method for investigating petroleum system elements (trap, seal, reservoir, etc.) of conventional and unconventional gas hydrate systems. BPSM enables the user to study gas hydrate by integrating geological knowledge, seismic information, and well data. The simulation of gas hydrate is coupled to the generation and migration of gas from the source and included in the material balance of the model. The gas hydrate stability zone is a sensitive system – accordingly, PetroMod enables users to determine the factors under which a gas hydrate stability zone can occur by applying PVT conditions as well as temporal and spatial refinement. The research project area of interest (AOI) is the Terrebonne Basin in the northern Gulf of Mexico (**Figure 1**). Inputs are determined from high-resolution USGS 2-D seismic lines, three wells in the AOI, and 3-D seismic that was depth converted using interpreted surfaces, two check-shot surveys, and interval velocities of wells.

The 3-D model (**Figures 2** and **3**) is composed of ~28 million cells and 128 layers at present day. Spatially, layers from seafloor to salt are as thin as ~0 ft due to sub-layering and pinch-outs. The total model size is 23,300 × 23,300 ft, or 466 × 466 grid cells, in the x and y directions. A mesh, with grid cells that are 50 ft × 50 ft, was used. From base of salt to seafloor, the model is, on average, 12,300 ft thick. Salt movement is determined by standard salt restoration methods (**Figure 4**). Erosion of up to ~1,000 ft (**Figure 5**) is interpreted and incorporated into the model as a regional angular unconformity. Temporally, 134 timesteps are simulated from 18 million years ago (Ma) to present with resolution of up to 900 years.

Lithologies are calibrated to porosity derived from a suite of well log curves using different percentages of sand, silt, shale, and marl, laterally and vertically (**Figure 6**). In addition, five pressure points from mud weights are used for calibration (**Figure 6**). The heat flow was determined by calibrating the base of the gas hydrate stability zone (BGHSZ) observed in 3-D seismic with the BGHSZ predicted by the model (**Figures 7** and **8**). Aside from lateral gas hydrate distribution correlation, the model output also matches well with vertical distribution of gas hydrate accumulations predicted by a suite of well log curves (**Figure 9**).

Hydrate recycling is observed in cross-sections and plan view of hydrate geobodies (**Figure 10**). Through time, a number of factors influence the evolution of hydrate accumulations and one of the driving mechanisms of initial hydrate formation is salt movement (**Figure 11**). With the calibrated 3-D model, we predict 1.32 TCF of methane gas is trapped as hydrate in this basin within both source and reservoir rocks. To put this in perspective, according to the U.S. EIA, last year 30 TCF of natural gas was consumed. One other published estimate, using interpretation of wells and seismic, of gas in-place in the form of hydrate in Terrebonne Basin is 744 BCF (Frye et al., 2012). Because only biogenic gas is simulated and the modeled hydrate saturations align vertically and laterally to those predicted by seismic and wells, we provide this study as support for the hypothesis that gas hydrate in this basin is of a predominantly – or perhaps nearly entirely – biogenic origin. Introducing a thermogenic source to the model may create larger discrepancy between the former estimate of gas volume trapped as hydrate and the estimate of this study.

This study is the first to: *(1)* integrate quantitative 3-D basin modeling of hydrate through time with erosion, *(2)* demonstrate that salt movement drives the initial formation of hydrate in a basin, *(3)* test the impact of thermal conductivity variations on the hydrate petroleum system which has implications for double BSR formation (a new hypothesis) and for drilling/well placement decisions beneath seismic resolution, *(4)* use 3-D basin models to test the effectiveness of hydrate as a trap and as a seal, *(5)* demonstrate that an angular unconformity driven by uplift and erosion results in formation of hydrate at updip pinchouts along the seafloor, and *(6)* use hydrate modeling as a way to predict fault behavior through time (e.g., when the fault is open versus closed).

Figures

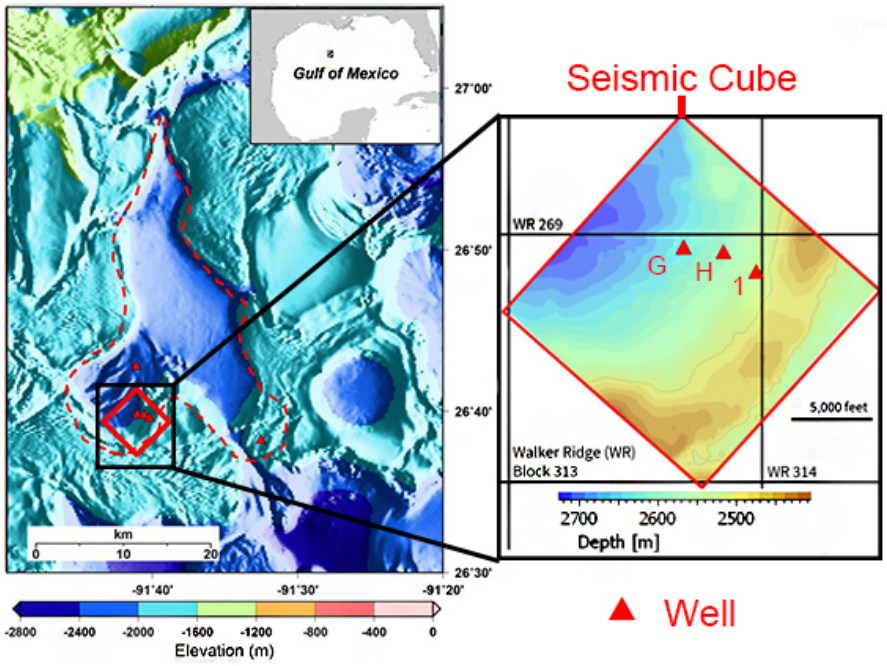

Figure 1. Location of Terrebonne Basin, Gulf of Mexico (red dashed line). Bold box outlines WR block 313, the region of a 3-D seismic cube used for model surfaces. Well locations with publicly available data shown by red triangles. Seafloor bathymetry at left from BOEM and at right from seismic.

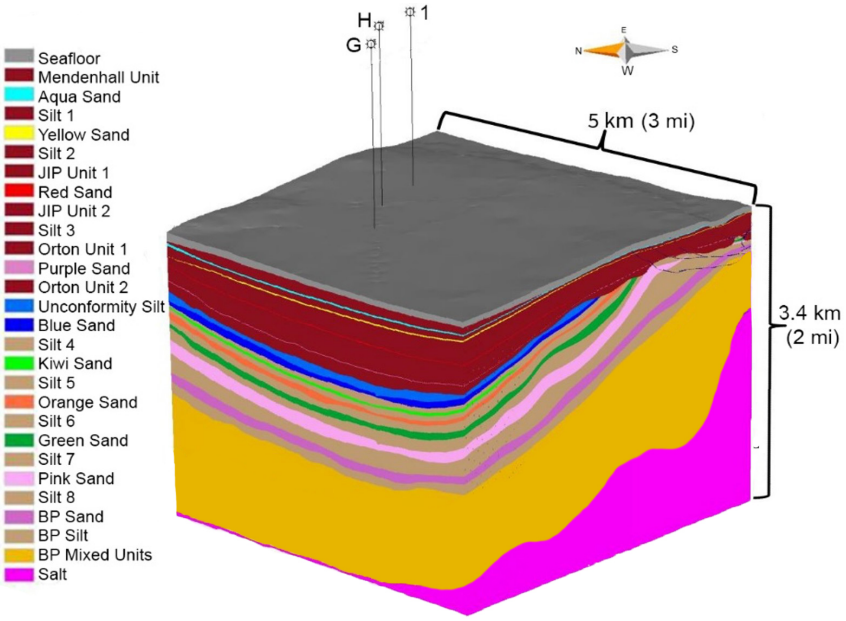

Figure 2. 3-D view of model surfaces. Seafloor through Pink Sand uses the naming convention established in literature, whereas BP Sand and deeper surfaces are interpreted using seismic and deep industry well #1.

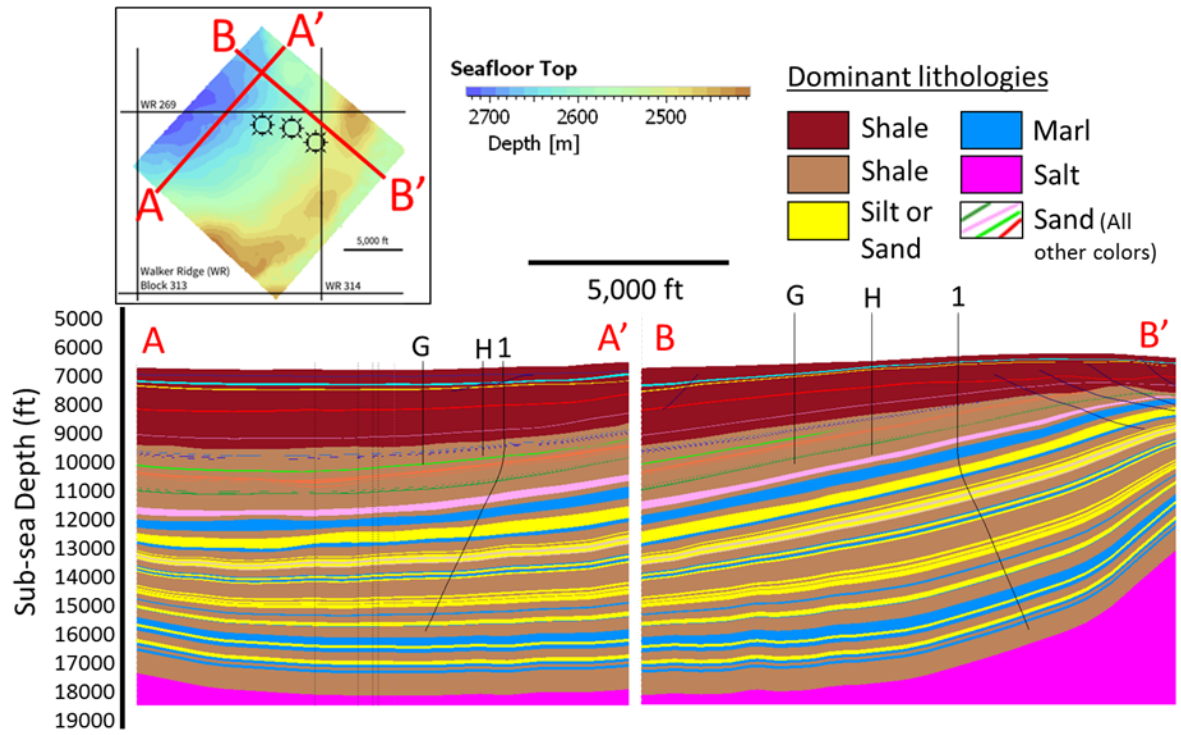

Figure 3. Cross sections from 3-D model. Dominant lithologies are displayed as well as projected wells and faults.

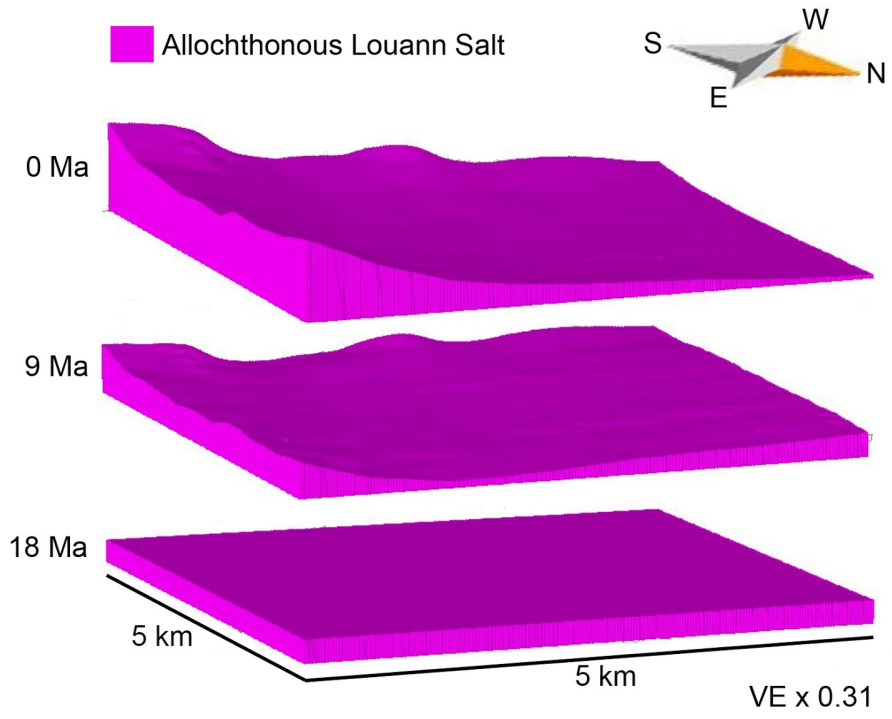

Figure 4. Reconstruction of salt 3D geometry through time. Salt volume = 15.42 km^3, average depth of 0 Ma surface = 6394 ft, VE = 0.31, uniform thickness of salt = 2024 ft.

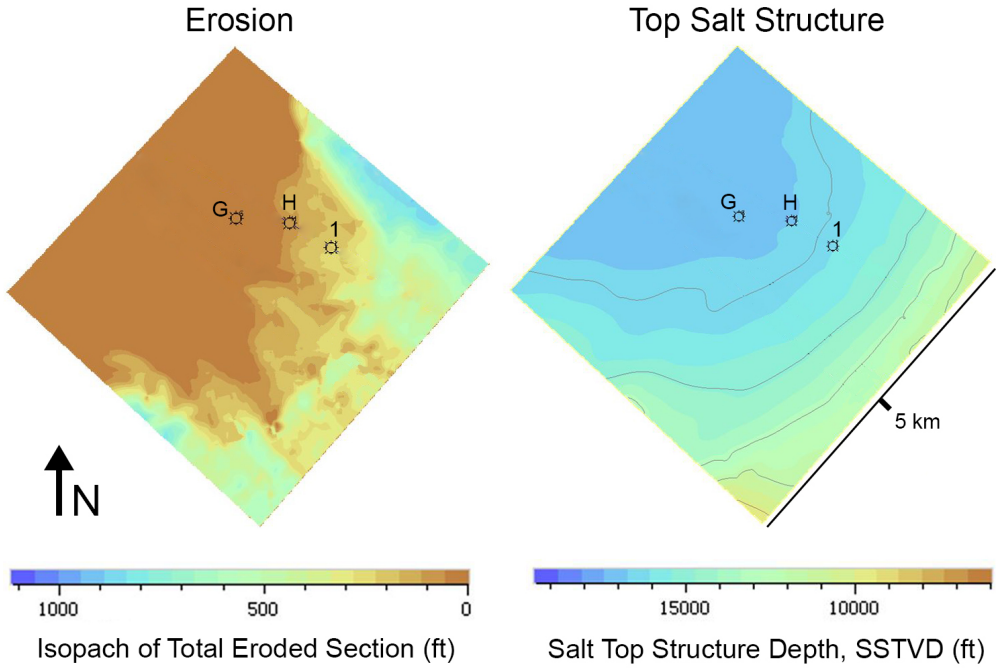

Figure 5. Erosion (interpreted from seismic) and salt structure exhibit similar crescent shaped geometry, implying a causal relationship.

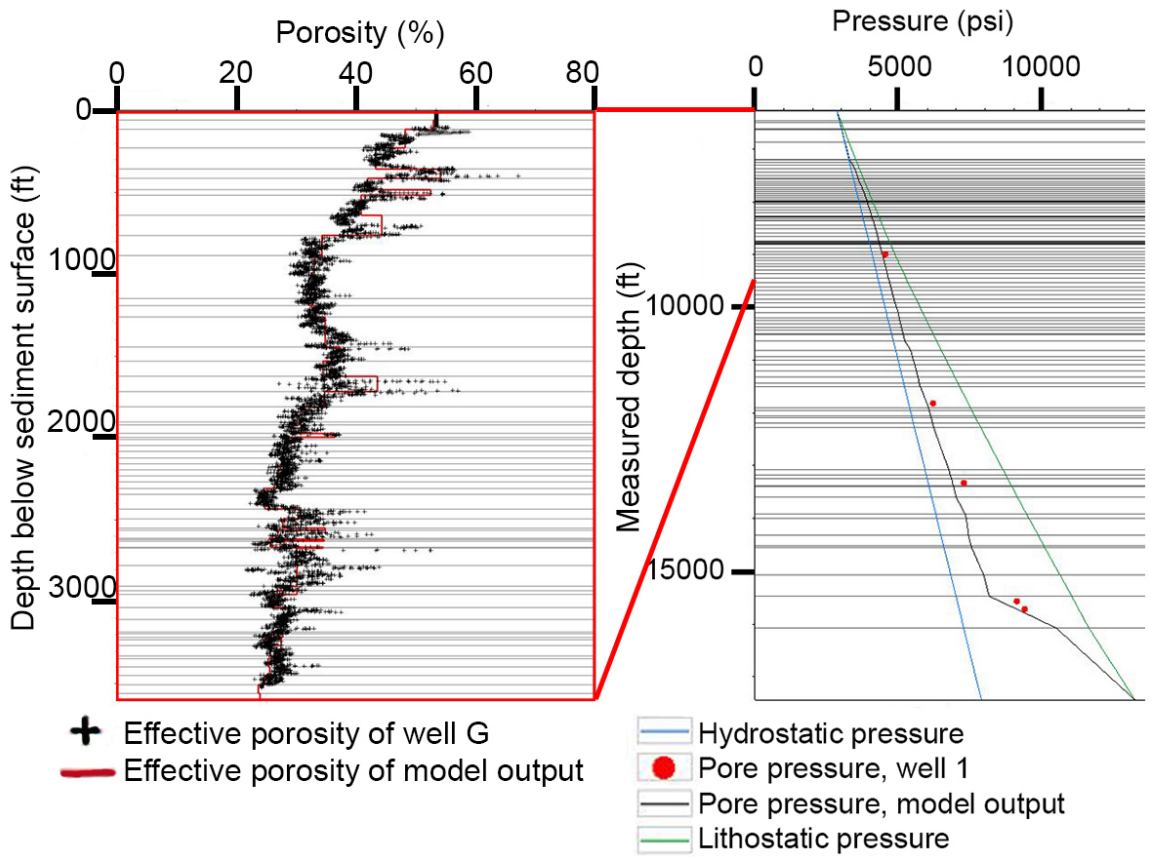

Figure 6. Porosity and pressure calibrations.

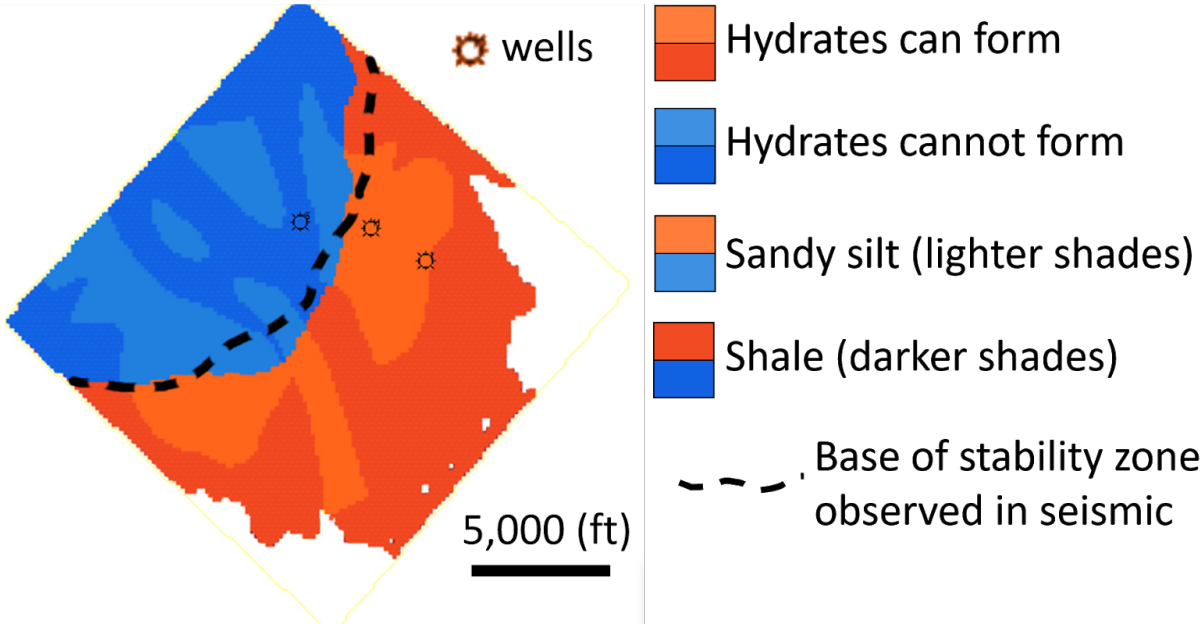

Figure 7. Hydrate accumulations in map view are predicted at key surfaces based on seismic attributes. Heat flow is the key controlling factor of the base of the gas hydrate stability zone.

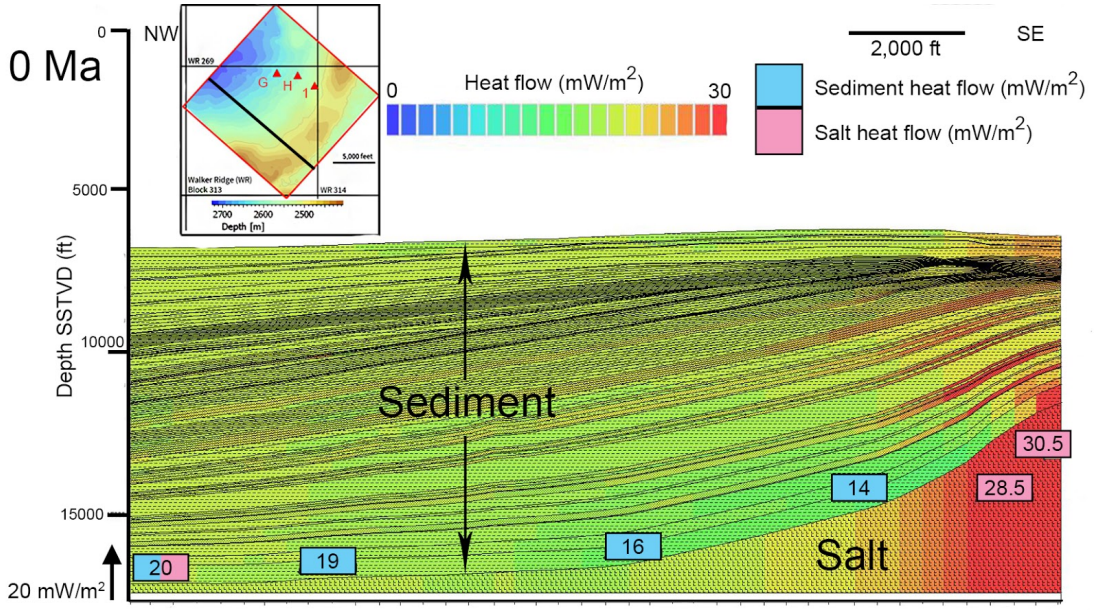

Figure 8. Cross-section of heat flow displays the influence of salt as it draws heat away from basin sediment and focuses it towards the top of the diapir.

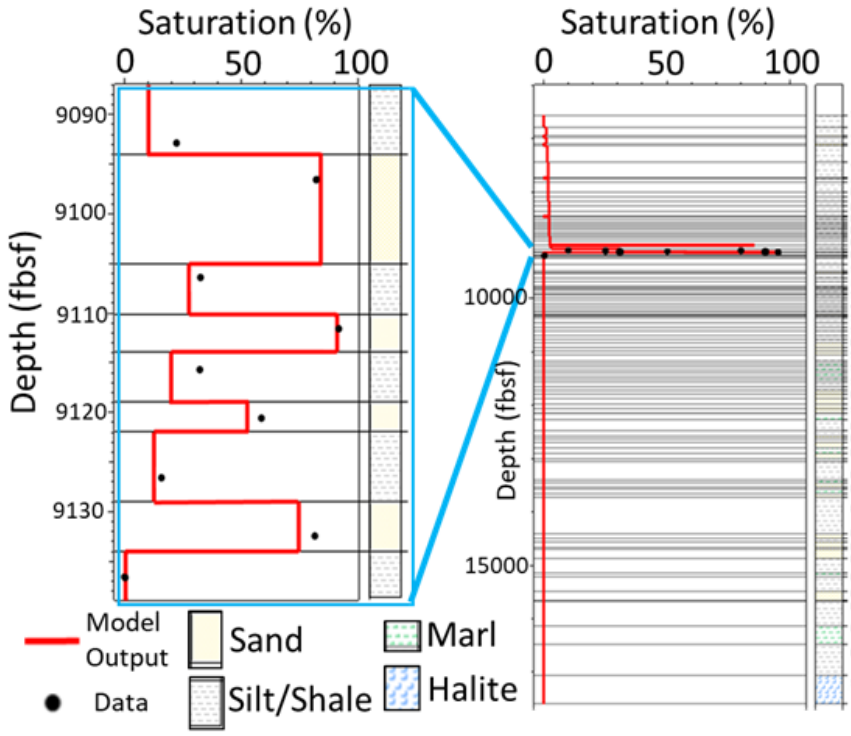

Figure 9. Modeled gas saturations agree well with saturations predicted from well logs.

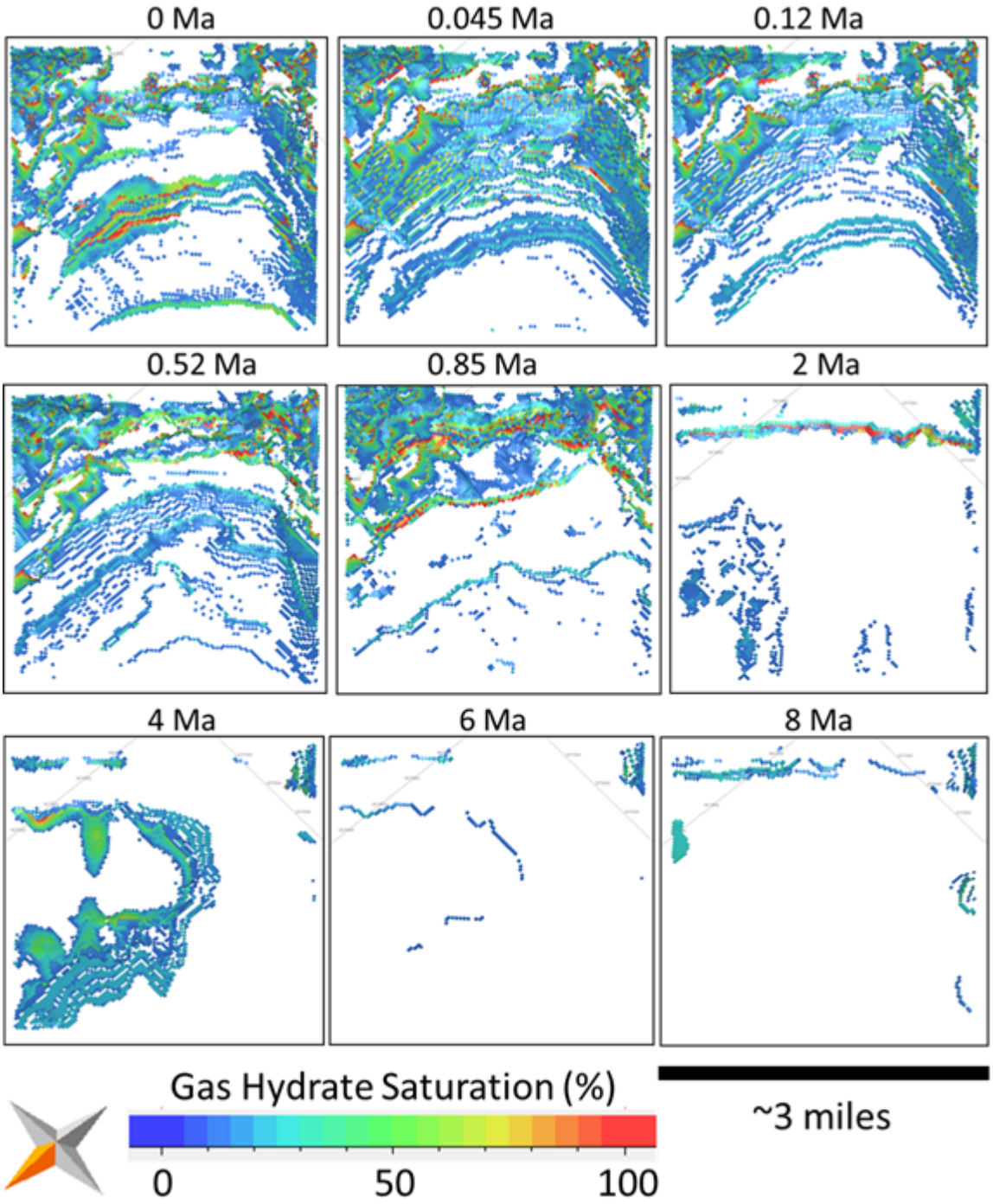

Figure 10. Model results of gas hydrate saturation through time. Nine timesteps from 8 Ma (the first occurrence of hydrate) to present (0 Ma) illustrate that highest saturation values and largest number of hydrate accumulations are at present day. Some accumulation geometries do not change through time.

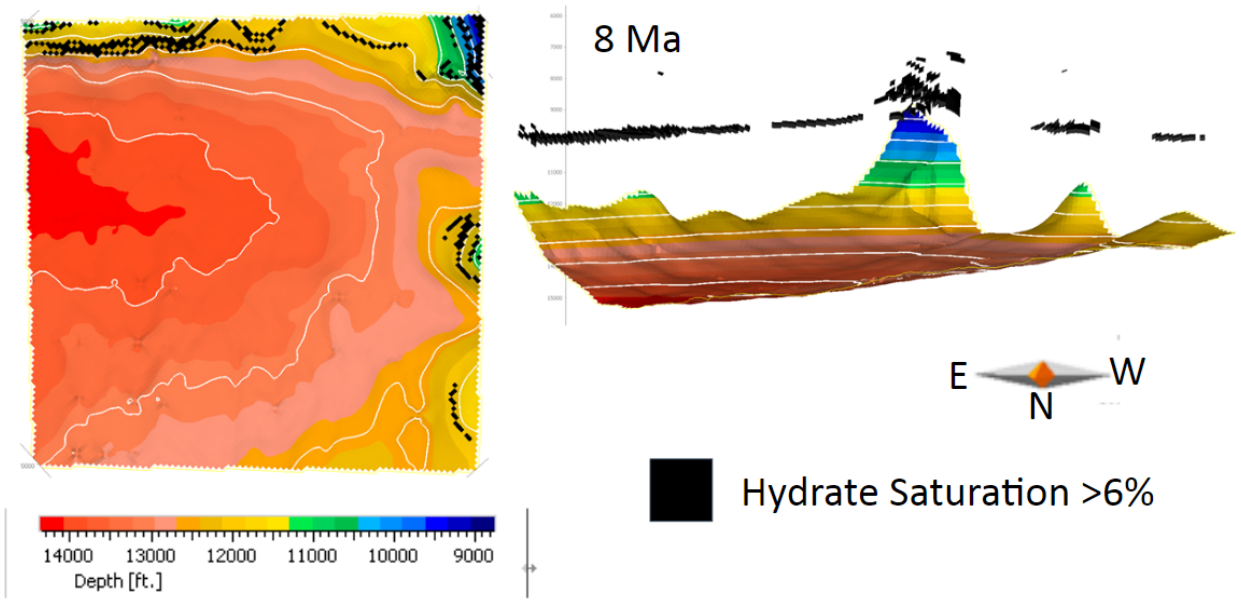

Figure 11. Plan view (left) and 3-D view (right) of top salt structure and hydrate accumulations. The model predicts that hydrate formed at 8 Ma was due to salt structure altering temperature. When salt evolved from a flat structure to one with variation in thicknesses, hydrate formed above crests of diapirs because increased temperature above diapir caused the stability zone to thin. This led to hydrate dissociation beneath the new stability zone, causing gas to migrate upwards and form higher hydrate concentrations at the new base of stability.

Acknowledgments

Special thanks to Oliver Schenk, Noelle Schoellkopf, and Les Magoon for helpful discussions and assistance. Value was added, in part via teachings and collaboration, by Yongkoo Seol, Wisam AlKawai, Mei Mei, Attila Bartha, Nour Koronful, Thomas Fuchs, Simone Salazar, Tim Collett, Ray Boswell, Tim McHargue, Anshuman Pradhan, Mustafa Al Ibrahim, Matt Frye, William Shedd, Kody Kramer, Stephen Palmes, Peter Flemings and his students, and Stewart Levin. We greatly appreciate Schlumberger for software, WesternGeco for data, and the DOE's National Energy Technology Laboratory for funding. Additional funding support for the first author has been awarded by Stanford's McGee/Levorsen Research Grant Program, Stanford's EDGE and SURGE, the AAPG, the Global Energy Forum, the Stanford Shell Fund, the Stanford Energy Club, and the Gordon Research Conference and Seminar on Natural Gas Hydrate Systems. The Basin and Petroleum System Modeling (BPSM) industry affiliates group at Stanford University supports this study.

References

Frye, M., W. Shedd, and R. Boswell (2012), Gas hydrate resource potential in the Terrebonne Basin, Northern Gulf of Mexico, Marine and Petroleum Geology, v. 34, i. 1, p. 150-168.

ANALYTICAL EQUATIONS FOR THE GROWTH OF CARBONATE PLATFORMS

Pulkit Singh[1*], Nicolas Goudemand[2], Jonathan Payne[1]
Fonctionnelle de Lyon, UMR 5242, 46 Allée d'Italie, F-69364 Lyon Cedex 07, France
[1]*Department of Geological Sciences, Stanford University, Stanford, CA, USA*
[2]*Univ. Lyon, ENS de Lyon, CNRS, Univ. Claude Bernard Lyon 1, Institut de Génomique*

Introduction

Carbonate platforms are unmatched repositories of our planet's physical, chemical, and biological evolutionary history (Wilson 1975; Grotzinger 1986, 1989). Carbonate reservoirs are also host to more than 60% of world's oil and 40% of world's gas reserves (Roehl and Choquette, 2012). One of the main challenges in exploring for hydrocarbons in carbonate systems is predicting the distribution of large-scale architectural elements like reefs and slope facies in carbonate platforms. Because carbonate platform deposits are inherently biological in nature, the growth patterns of reefs and platforms are controlled by the dominant ecology. Predicting these growth patterns is essential in carbonate reservoir exploration as the growth patterns control facies distribution and internal stratigraphic architecture of the carbonate platforms. The distribution of facies is the principal control on the distribution of porosity and permeability properties of carbonate reservoirs. For instance, fine grained carbonate mudstone gives rise to intergranular and intercrystalline porosity, whereas grainstone and packstone facies give rise to moldic or solution enlarged cavernous porosities. Various forward stratigraphic modeling techniques have been used to simulate carbonate platform evolution as a function of sediment production, transport, tectonic subsidence, and eustasy. However, modeling the complex interaction between these physical factors generally leads to nonlinear sets of equations that are not only inherently complex to solve but also prohibit the complete exploration of parameter space. Another associated challenge is the non-uniqueness of the input parameters incorporated while modeling carbonate dominant sedimentary systems. We have developed a suite of analytical equations that are computationally inexpensive, reduce the non-uniqueness problem, and allow comprehensive exploration of parameter space while modeling the petroleum systems involving carbonate sedimentary systems.

Methodology

Geometrically, an attached carbonate platform is distinguished by a flat inner platform abruptly transitioning into relatively steeper slope environment and into the adjacent basin (**Figure 1**). The platform geometries are categorized as prograding, aggrading, or retrograding based on the changing position of the platform margin through time (Read, 1982). We assumed an initial platform geometry and using simple assumptions about subsidence, sediment production, and transport, we developed analytical equations that predict the evolution of platform geometries. In case where the margin trajectory is available from seismic and/or outcrop data, we calculate basin modeling parameters such as sediment production rate. We also limit the sediment transport width of the platform by

using an inverse modeling approach. Finally, we modeled the impact of basinal/pelagic sedimentation on the evolutionary trajectory of the carbonate platforms (**Figure 2**).

Results and Conclusions

We modelled the interactions between antecedent topography, nature of carbonate factory (reef vs microbial), and sediment transport width to predict the evolution of carbonate platform trajectories.

To test the practical applicability of our growth equations, we applied our model equations to the Carboniferous Sierra Del Cuera carbonate platform (microbial factory) in Spain and Llucmajor Reef complex in Mallorca (**Figure 3**) to inversely calculate platform parameters like sediment production potential and sediment transport width. These inversely calculated parameters are geologically constrained and can be used as basin modeling inputs while developing complex reservoir models for carbonate platforms with microbial factory (Ex. Tengiz Field, Kazakhstan) or with metazoan reef factory (Ex. Miocene carbonate complexes in central Luconia, Malaysia).

In conclusion, our models reliably predict the growth trajectories of carbonate platform margins using the simple assumptions about subsidence, pelagic sedimentation, sediment production, and transport. These models alleviate the problem of non-uniqueness and allow for comprehensive exploration of parameter space while modeling the stratigraphic evolution of carbonate sedimentary systems.

References

Grotzinger, J.P., 1986. Cyclicity and paleoenvironmental dynamics, Rocknest platform, northwest Canada. *Geological Society of America Bulletin*, *97*(10), p. 1208-1231.

Grotzinger, J.P., 1989. Facies and evolution of Precambrian carbonate depositional systems: emergence of the modern platform archetype. in Crevello P. D., Wilson J. L., Sarg J. F. and Read J. F. eds., *Controls on Carbonate Platform and Basin Development SEPM Special Publication* 44, p. 79-106.

Read, J.F., 1982, Carbonate platforms of passive (extensional) continental margins: types, characteristics and evolution: *Tectonophysics*, v. 81, p. 195-212

Roehl, P.O. and Choquette, P.W. eds., 2012. *Carbonate petroleum reservoirs*. Springer-Verlag, New York, 622 p.

Wilson, J.L., l., 1975, *Carbonate facies in geologic history*. Springer Verlag, New York, 471 pp.

Figures

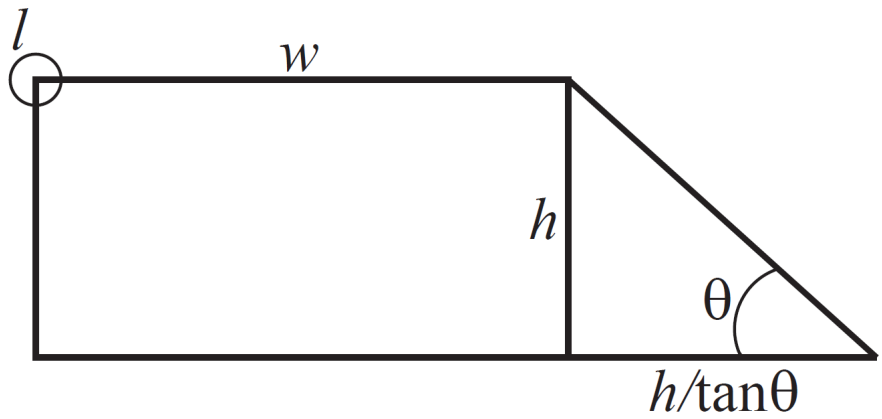

Figure 1. The initial platform geometry assumed for carbonate platform.

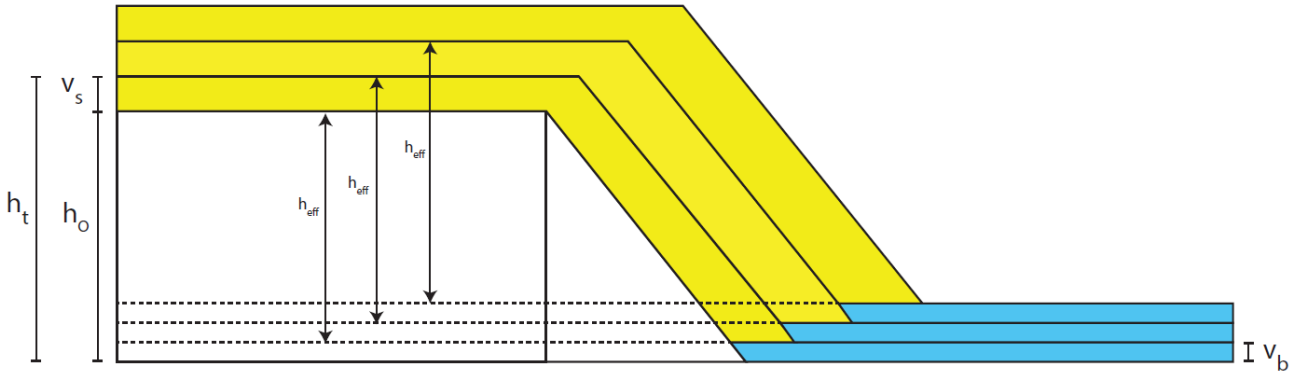

Figure 2. The figure above shows the modeling approach used to model the influence of pelagic sedimentation on the evolution of platform trajectories.

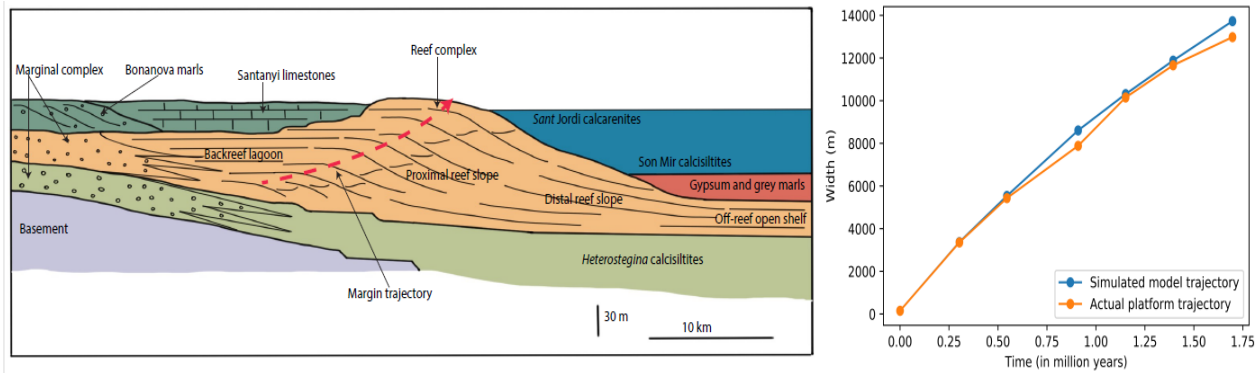

Figure 3. The figure on the left shows the margin trajectory (dashed red line) of the Llucmajor Reef complex and the figure on the right shows the simulation results of the modeled vs actual platform geometry.

PREDICTING DEPOSITIONAL INTERPARTICLE POROSITY OF OOLITE USING OOID SIZE

Xiaowei Li[1] and Jonathan L. Payne[1]
[1]Department of Geological Sciences, Stanford University, Stanford, CA 94305
xwli@stanford.edu; jlpayne@stanford.edu

Abstract

Oolite can develop into economically profitable hydrocarbon reservoirs. Examples include the Lower Triassic Khuff Formation in the Middle East, the Feixianguan Formation in south China, and the Jurassic Smackover Formation in the United States. Predicting the reservoir quality of oolite is one of the main challenges for petroleum exploration because depositional porosity can be overprinted by complex diagenetic processes. Core analysis techniques and wireline logs (density, sonic, neutron and NMR logs) are useful tools for reservoir characterization, but they do not directly reveal the controls on reservoir quality that are critical for prediction away from the wellbore. As a solution, forward diagenetic models have been used to predict reservoir quality in undrilled locations. Among initial input parameters, depositional porosity is a critical one at influencing final modeling results.

Interparticle porosity is the most important type of primary porosity in oolite. Interparticle pores in oolite are primarily influenced by the sizes of ooids and the amount of early marine cements occluding pores (**Figure 1**). Ooid sizes vary substantially in space and in time. Modern ooids typically have diameters in the range of 0.5 mm and ancient ooids are typically smaller than 2 mm in diameter, but ooids approaching or even exceeding 10 mm in diameter occur in Neoproterozoic and Lower Triassic marine carbonate succession (Sumner and Grotzinger, 1993; Lehrmann et al., 2012).

The size of ooids can be predicted from carbonate saturation state in the water column and transport intermittency of ooids through a physio-chemical model (Trower et al., 2017). In general, higher carbonate saturation state tends to increase ooid size by elevating precipitation rate whereas greater transport intermittency tends to reduce the size by escalating time-averaged abrasion rate (**Figure 2**). Transport intermittency of ooids would be related to transport distance from their original site of precipitation (i.e., oolitic shoals on platform margin), likely reflecting increasing distance from platform margin and changes in depositional sub-environments (e.g. back-shoal versus channels between oolitic bars). In addition to controlling the size of ooids, coeval carbonate saturation state also directly determines the rate of carbonate mineral precipitation (Burton and Walter, 1987) and therefore the amount of early marine cements filling the interparticle pores among ooids (**Figure 1**). This relationship implies that the amount of early marine cements can be estimated and predicted if the size of ooids is known at different sub-environments. Thus, the depositional interparticle porosity in oolite can be further quantified for oolite deposited away from platform margin.

The Great Bank of Guizhou is a Permian-Triassic isolated carbonate platform in the Nanpanjiang Basin of south China. It transitioned from a low-relief, gently dipping carbonate ramp from the earliest Triassic to a high-relief, steep-sloped carbonate platform before the Middle Triassic without microbial and metazoan reefs and synsedimentary tectonics near platform margin (**Figure 3**). During the transition, oolite was the main lithofacies on the platform margin and occasionally extended to platform interior. Because its stratigraphic architecture is well exposed by a platform-to-basin transect (**Figure 3**), it offers a rare opportunity to test the potential relationships among carbonate saturation state, ooid size, amount of early marine cements, and depositional interparticle porosity in oolite with distance to the platform margin.

Future work will focus on quantifying the size distribution of ooids and amount of early marine cements at different locations along the same bed or interval of oolite away from platform margin. Results from this study might shed light on prediction of depositional interparticle porosity in oolite for forward diagenetic modeling and improve the precision of simulations prior to drilling.

Figures

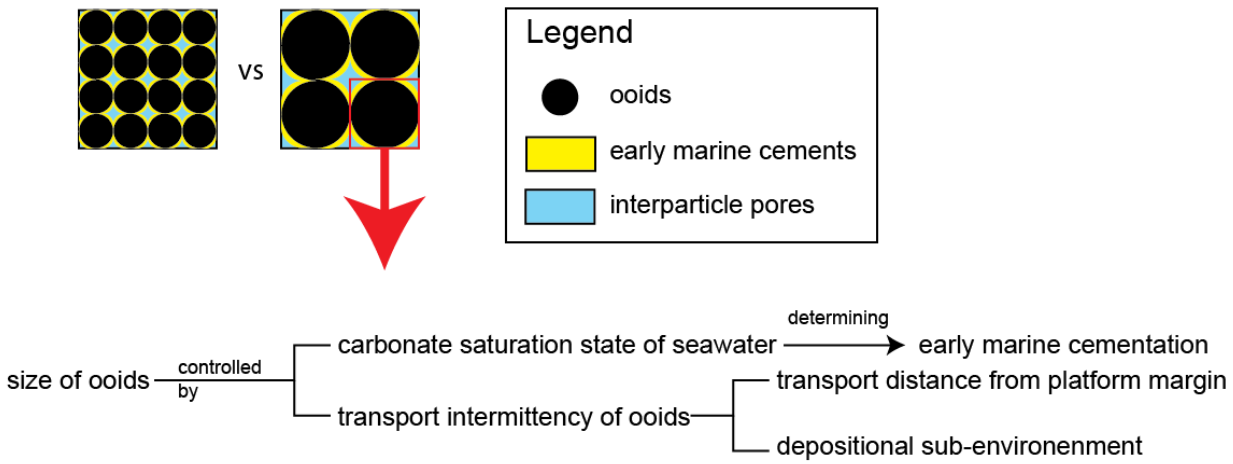

Figure 1. Porosity controlled by different sized ooids and relationship between carbonate saturation state, ooid size, and early marine cementation.

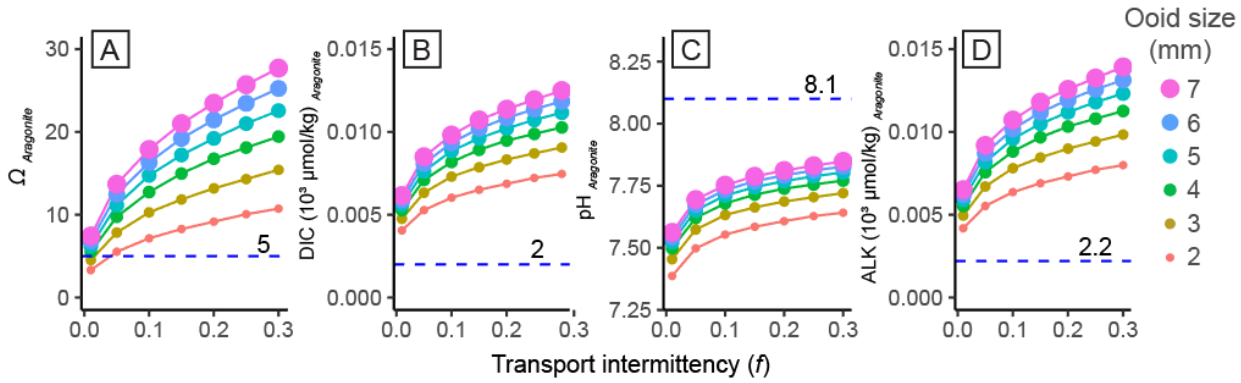

Figure 2. Modeling results of chemical properties of seawater carbonate chemistry required for Early Triassic giant ooid (>2mm) formation in the Great Bank of Guizhou. Dashed lines represent values from modern tropical ocean.

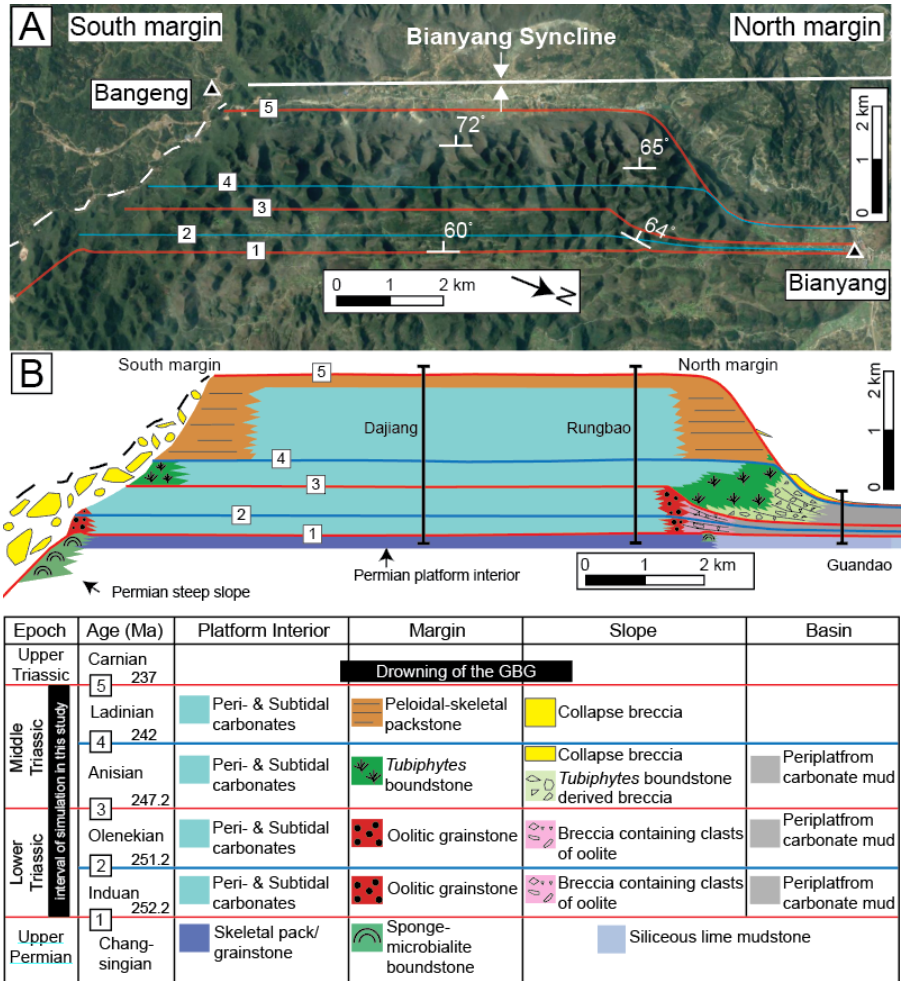

Figure 3. Satellite image and stratigraphic architecture of the Great Bank of Guizhou.

References

Burton, E.A., Walter, L.M., 1987. Relative precipitation rates of aragonite and Mg calcite from seawater: Temperature or carbonate ion control? Geology 15, 111–114. https://doi.org/10.1130/0091-7613(1987)15<111:RPROAA>2.0.CO;2

Lehrmann, D.J., Minzoni, M., Li, X., Yu, M., Payne, J.L., Kelley, B.M., Schaal, E.K., Enos, P., 2012. Lower Triassic oolites of the Nanpanjiang Basin, south China: Facies architecture, giant ooids, and diagenesis-implications for hydrocarbon reservoirs. Am. Assoc. Pet. Geol. Bull. 96. https://doi.org/10.1306/01231211148

Sumner, D.Y., Grotzinger, J.P., 1993. Numerical modeling of ooid size and the problem of Neoproterozoic giant ooids. J. Sediment. Petrol. 63, 974–82. https://doi.org/10.1306/D4267C5D-2B26-11D7-8648000102C1865D

Trower, E.J., Lamb, M.P., Fischer, W.W., 2017. Experimental evidence that ooid size reflects a dynamic equilibrium between rapid precipitation and abrasion rates. Earth Planet. Sci. Lett. 468, 112–118. https://doi.org/10.1016/j.epsl.2017.04.004

MODELING PETROLEUM EXPULSION AND RETENTION FROM SOURCE ROCKS WITHIN THE VACA MUERTA FORMATION, NEUQUÉN BASIN, ARGENTINA

Mei Mei[1, *], Alan Burnham[1], Noelle Schoellkopf[2], Tapan Mukerji[1], Johannes Wendebourg[3], Francois Gelin[4]
[1]*Department of Energy Resources Engineering, Stanford University, CA, USA*
[2]*Department of Geological Sciences, Stanford University, CA, USA*
[3]*TOTAL E&P Americas, Houston, TX, USA*
[4]*TOTAL E&P Research & Technology, Pau, France*
[*]meimeisu@stanford.edu

Abstract

Improved understanding and prediction of overpressure, porosity, thermal history, and petroleum expulsion, retention, and producibility from source rocks was achieved through advanced 3D basin modeling, integrating compositional kinetics, geochemistry, and geomechanics of the Vaca Muerta Sequences, Neuquén Basin, Argentina. The source rock data show lateral and vertical heterogeneities. The effects of key mechanisms and variables were studied, such as the compressibility, permeability-porosity relationship, facies heterogeneity, erosion and maturation timing, heat flow history, kerogen reaction kinetics, and petroleum adsorption within the source rock. The 3D basin model was calibrated with a multidisciplinary dataset. Model results indicate that basin-wide petroleum expulsion likely started in the late Cretaceous (**Figure 1**), when active primary and secondary petroleum generation exceeded the retention capacity of the source rock and associated pore pressure exceeded the hydraulic fracturing threshold (**Figure 2**). Expulsion likely ceased in stages during the Early Tertiary until the Mid-Miocene when pore pressure decreased due to the completion of primary generation and cracking of polar components, secondly cracking of saturates and aromatics, and finally cracking of wet gas components. Through continuous burial and thermal maturation, cracking continued until the final products of coke and methane, whereas petroleum retention decreased due to expulsion and decreased retention capacity of coke compared to active kerogen.

Geological evidence and modeling indicate that tectonic uplift likely started in the mid-Miocene (~15 Ma), which relaxed thermal stress and pore pressure and terminated secondary cracking (**Figure 2**). Model results also suggest that during the thermal maturation process, adsorbed hydrocarbons always exceed free hydrocarbons retained in the source rock (**Figure 1**). The modified 14 component kinetics and adsorption model have similar reaction and adsorption framework as Burnham (2017b) for cokes, polar components, light and medium saturates and aromatics, wet gases, methane, carbon dioxide, and water. After calibration of kerogen reaction kinetics, cracking kinetics for 10 secondary reactants and 12 byproducts, and the preferential capacities of adsorption for 14 components, free hydrocarbons in the source rock pore space have similar composition to produced oils, and total retained (adsorbed and free) oil has a similar composition to rock extracts (**Figure 3**).

The basin model indicates that (1) polar components are preferably adsorbed in source rock at <0.75%Ro, then cracked throughout maturation, and mostly consumed by about 1.40%Ro; (2) At <1.15%Ro, saturates and aromatics are generated in about equal proportion and stored within the source rock; (3) Saturates gradually increase relative to aromatics in both free and adsorbed oil due to preferential generation of saturates by thermal cracking and preferential thermal cracking of aromatics, which are mostly consumed by about 1.65%Ro; (4) the preferential adsorption of aromatics causes a higher saturates-to-aromatics ratio in the free oil. The model for a closed system predicts that further maturation would consume residual oil (light saturates) by 2.60%Ro; and that wet gas components would be depleted by 3.35%Ro. The methodology and the insights of this study not only improve the fundamental understanding of petroleum expulsion and retention within the Vaca Muerta Formation, but also can be applied to global unconventional oil and gas plays.

Figures

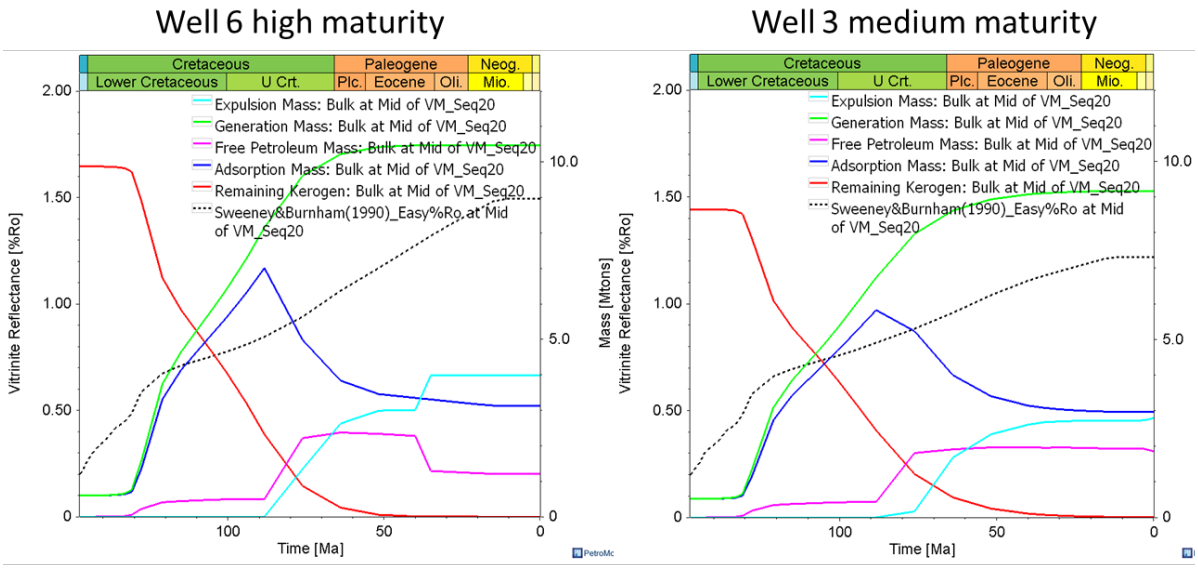

Figure 1. Maturation, petroleum generation, retention, and expulsion histories for wells with different thermal maturities.

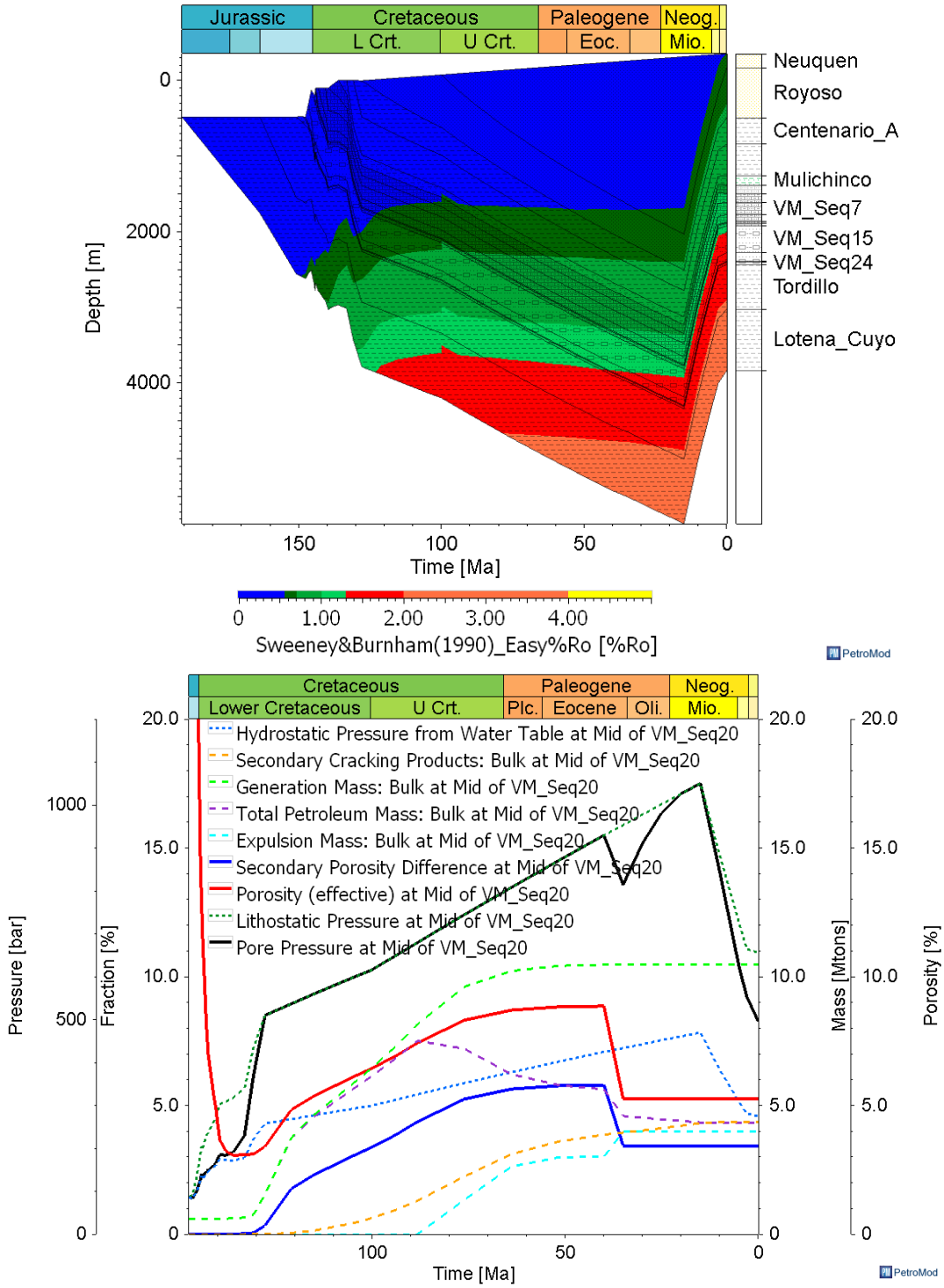

Figure 2. Burial history and associated pressure, porosity, and petroleum histories for well 6.

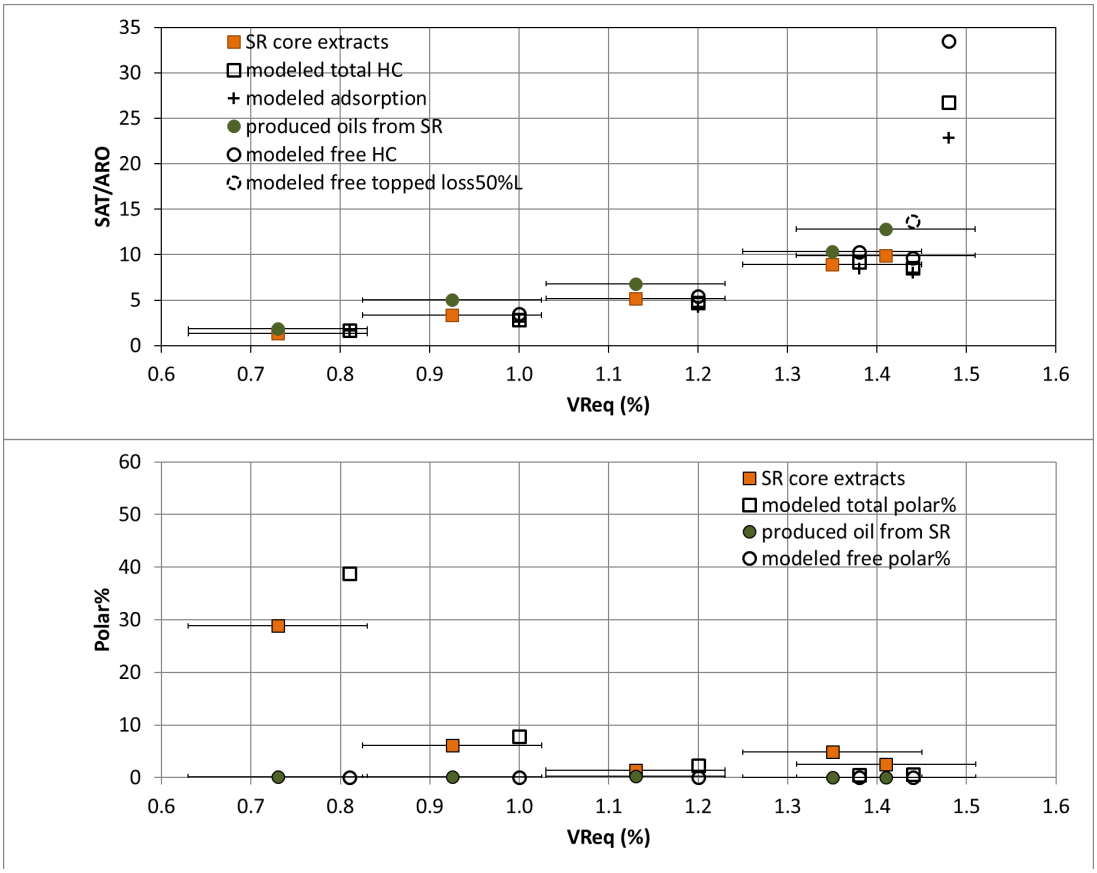

Figure 3. Comparison of modeling results and measured data for polar percent and saturates-aromatics ratio (Sat/Aro) vs. vitinite reflectance equivalents VReq (%).

Acknowledgments

We thank Total Exploration & Production, Unconventional Research & Development Program for funding, datasets, and technical support. We appreciate advice from L. B. Magoon, A. Hosford Scheirer, K. E. Peters, S. A. Graham, and J. M. Moldowan at Stanford University and advice from T. Hantschel, O. Schenk, T. Fuchs and the technical support team at Schlumberger. Thank you to Schlumberger for PetroMod software.

References

Burnham, A. K. Global Chemical Kinetics of Fossil Fuels: How to Model Maturation and Pyrolysis. Springer: Cham, Switzerland, 2017.

Burnham, A. K. and Braun, R. L., 2017. Simple Relative Sorptivity Model of Petroleum Expulsion. Energy & Fuels 31, 9308-9318, 2017.

Hantschel, T. and Kauerauf, A. I. Fundamentals of Basin and Petroleum Systems Modeling. Springer: Berlin, Heidelberg, 2009.

THREE-DIMENSIONAL BASIN AND PETROLEUM SYSTEM MODELING AS AN INVESTIGATIVE TOOL FOR THE EVOLUTION OF SOURCE ROCK THERMAL MATURITY IN THE MIDDLE MAGDALENA VALLEY, COLOMBIA

William Thompson-Butler[1,*], Allegra Hosford Scheirer[1], Noelle B. Schoellkopf[2], Leslie B. Magoon[1], and Stephan A. Graham[1]

[1]*Department of Geological Sciences, Stanford University, Stanford, CA*

[2]*Schlumberger, Mill Valley, CA, 94941*

[*]rthomps@stanford.edu

Abstract

The Middle Magdalena Valley (MMV) is an intermontane basin and petroleum province in northern Colombia that, along with the Eastern Cordillera and Llanos Basin, acted as a regional sedimentary basin from the Triassic into the Late Neogene (**Figure 1**). The MMV is a productive petroleum province, accounting for nearly 3 billion barrels of oil and 3 trillion cubic feet of gas from more than 40 fields in over a century of exploration (IHS, 2010). The distribution of fields, in addition to the estimated ultimate recoverable resource in oil equivalent barrels, are shown in **Figure 2**. Several of the larger accumulations in the central portion of the study area were discovered early in the basin exploration history (Morales, 1956; Dickey, 1992). However, as exploration progressed, large fields in the southern portion of the MMV, as well as several moderate to small accumulations in the northern MMV, have contributed to reserves. Despite this long history of petroleum exploration, the complex burial and variable exhumation history associated with the Andean orogeny contribute uncertainty to the evaluation of petroleum systems in the MMV by affecting the distribution, quality, and thermal maturity of the thick Cretaceous interval of organic-rich source rocks.

During the Late Cretaceous, restricted marine conditions resulted in deposition of organic-rich carbonate and siliciclastic sediments in a broad foreland basin within the MMV, Llanos Basin, and the modern-day Eastern Cordillera (Cooper et al., 1995; Parra et al., 2009; Villamil, 1999). The generative potential of the Upper Cretaceous La Luna Formation, a lateral equivalent to the primary source rock of the same name for the Maracaibo Basin in Venezuela, has been well-documented through source rock analysis and oil-source rock extract correlations within the MMV (e.g., Zumberge, 1980, 1984; Ramon et al., 2001; Rangel et al., 2000). However, other source rocks could also contribute to change in the basin. Specifically, deposition of the Aptian-Albian Tablazo Formation was coincident with a period of ocean anoxia and local deepening that resulted in organic matter preservation (Villamil, 1998).

A regional study of Colombian oils by Rangel et al. (2017) identified two petroleum families in the MMV and suggested that one originated from the calcareous facies of the La Luna Formation, whereas the other originated from siliciclastic facies of the Tablazo Formation. An oil-source rock correlation performed by Rangel et al. (2002) identified petroleum in the MMV from the transitional Umir Formation, stratigraphically above the La

Luna, as well. **Figure 3** shows a log suite of Rock-Eval T_{max} (the temperature corresponding to the maximum production of hydrocarbon products by kerogen cracking during pyrolysis), resistivity, total organic carbon (*TOC*), and hydrogen index (*HI*) data for a location in the central MMV. The erosion of the Lisama and Umir formations as well as the Olini Member of the La Luna Formation illustrate the impact in the central MMV of the Eocene exhumation. The source potential of the interval is also illustrated by the high *TOC* and resistivity values of the La Luna and Tablazo formations. However, the elevated thermal maturity, indicated by Rock-Eval T_{max}, and resulting depletion of *HI* in the Tablazo Formation complicate the thermal maturation and petroleum system story. In so doing, the log in **Figure 3** illustrates both the source potential of the Cretaceous interval within the MMV and the importance of modeling thermal maturation in understanding the resulting petroleum systems.

Plate convergence along the western margin of South America acted as the primary driver for the Paleogene evolution of the MMV. The oblique accretion of the Panama arc and the western terranes of the Central and Western Cordilleras propagated deformation from the Central Cordillera eastward. In the process, tectonic inversion of the Mesozoic rift system in the present-day Eastern Cordillera fragmented the once continuous foreland basin and exhumed Paleocene and Late Cretaceous sediments of the MMV (Parra et al., 2009; Restrepo-Pace et al., 2004; Mora et al., 2009). During this period, the environment of deposition in the MMV transitioned to nonmarine with intervals of fluvial and alluvial fan sandstones denuded from exhumed intervals in the flanking cordilleras (Reyes-Harker et al., 2015). Most oil and gas fields in the MMV produce from the Paleogene fluvial-sandstone reservoirs of the Colorado, Mugrosa, Esmeraldas, and La Paz Formations. However, new play concepts targeting Cretaceous siliciclastic reservoirs are being explored (e.g. Prince et al., 2011). Three-dimensional basin and petroleum system modeling (BPSM) can be used as a tool for the integration of research and data from past academic and industry work in order to address unanswered questions surrounding the complex interplay of the MMV's basin evolution and petroleum systems.

The objectives of this study are to: (1) understand source rock thermal maturation through time; (2) incorporate the effects of the Eocene exhumation and subsequent reburial on thermal maturation; and (3) relate the three-dimensional modeling results to the geochemically distinct petroleum tribes within the basin (Thompson-Butler et al., 2019).

Data from 250+ wells were used to construct a three-dimensional basin and petroleum system model for the Middle Magdalena Valley (MMV), Colombia. Twenty-five geologic layers are used to capture the Jurassic - to - modern sedimentary units deposited within the MMV. Twenty-six one-dimensional models were used to predict the variable eroded thickness related to the early Eocene exhumation across the basin and models were calibrated to thermal maturity and temperature data. Six distinct source rock intervals – the Tablazo Formation, Salada, Pujamana, Galembo, and Olini Members of the La Luna Formation, and the Umir Formation – were defined and populated with unique TOC and HI maps and kinetics. The present-day modeled transformation ratio (TR) indicates that much of the Tablazo Formation is in the late oil window to overmature whereas the Salada and

Pujamana Members of the La Luna Formation are in the late oil window in the northern, eastern, and southern basin depocenters. In contrast, the Galembo Member and, to a larger extent, the Olini Member and Umir Formation, are in the early to peak generative window in much of the basin. Additionally, modeled bulk petroleum generation over time shows that the majority of petroleum generation in the basin since early Eocene exhumation has come from these three intervals as tectonic accommodation along the eastern flank of the basin resulted in the deposition of thick Miocene overburden. Despite peak-to-late oil window thermal maturities in sections of the present day Tablazo, Salada, and Pujamana intervals, these units have been inactive for petroleum generation in much of the basin since the early Eocene. Capturing the variability in thermal maturation and petroleum generation over time within the Cretaceous source rock intervals illustrates the value of BPSM in petroleum system analysis of the MMV.

Figures

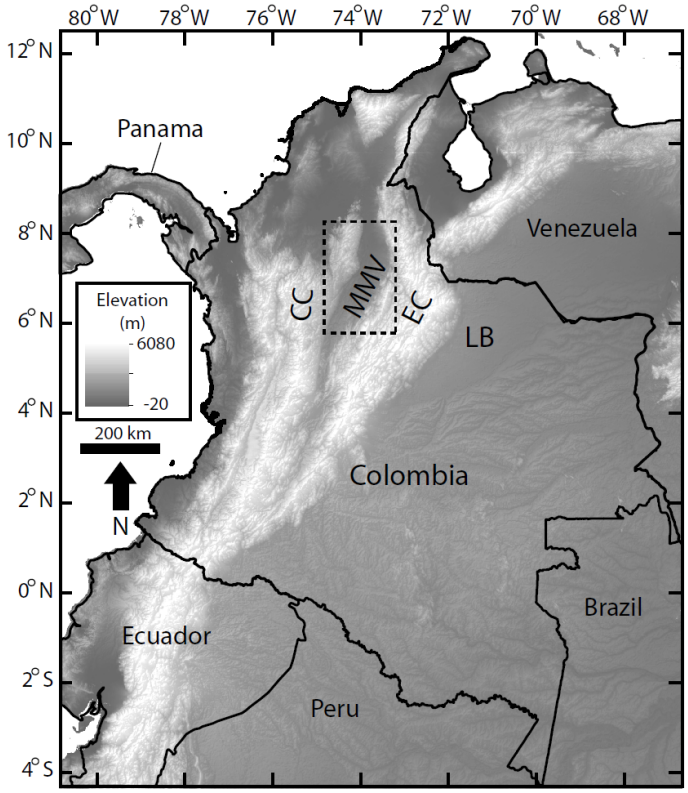

Figure 1. Elevation map of Colombia showing the location of the Middle Magdalena Valley (MMV) in the dashed black inset box. In addition, the Central Cordillera (CC), Eastern Cordillera (EC), and Llanos Basin (LB) are labeled.

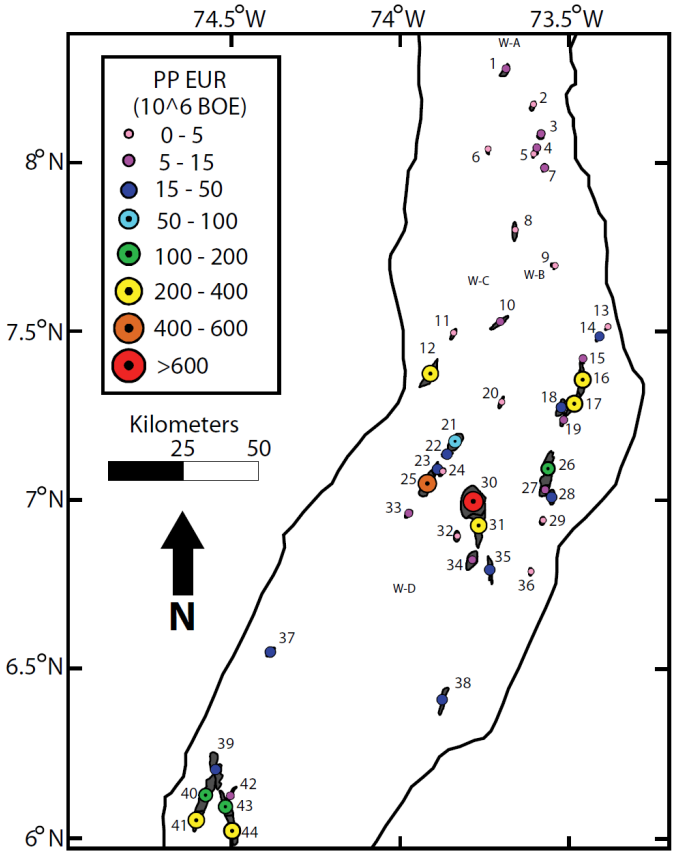

Figure 2. Map of the Middle Magdalena Valley, roughly the area of the inset box in **Figure 1**. The location of oil fields and four wells with fluid samples used in Thompson-Butler et al., 2019 (W-A to W-D) are shown. Circle sizes indicated the proven probable estimated ultimate recovery in 10^6 barrels of oil equivalent (BOE) for each field (IHS, 2010; internal Ecopetrol reporting). Numeric labels are used as map identifiers referenced in Table 1. EUR = estimated ultimate recovery; PP = proven probable.

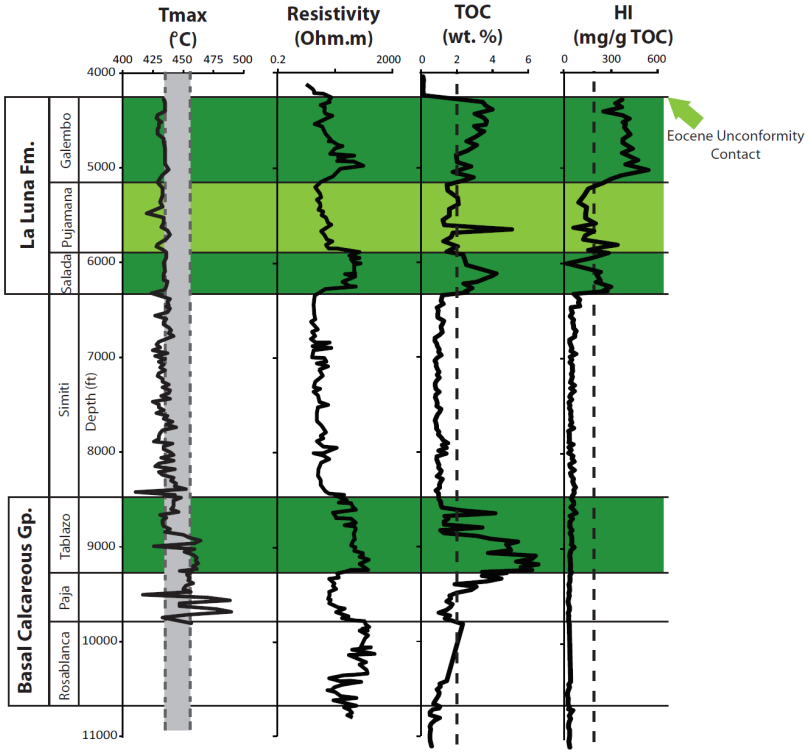

Figure 3. Geochemical log of Rock-Eval T_{max}, resistivity, total organic carbon (*TOC*), and hydrogen index (*HI*) for the Cretaceous section in a well in the central Middle Magdalena Valley. Dashed lines indicate threshold values of T_{max} (435°C and 455°C), *TOC* (2 wt. %), and *HI* (200 mg/g *TOC*). The Eocene unconformity shows that the Lisama Formation, Umir Formation, and the Olini Member of the La Luna Formation are eroded. Primary source intervals, dark green, local source rock intervals, light green. Fm., Formation; Gp., Group.

Acknowledgments

I would like to thank Ecopetrol for providing the data and analyses for this study and for permission to use it as part of my dissertation and Schlumberger for providing a license and support for PetroMod software. Special thanks go to Kenneth Peters, Mike Moldowan and Roman Eugenio Gonzalez for valuable discourse that improved the quality of this manuscript. Additional thanks go to the members and affiliates of the Basin and Petroleum System Modeling Group at Stanford (http://bpsm.stanford.edu) for support throughout this project.

References

Cooper, M. A., et al., 1995, Basin development and tectonic history of the Llano basin, eastern Cordillera and middle Magdalena valley, Colombia, AAPG Bulletin, v. 79, p. 1421-1443.

Dickey, P., 1992, La Cira-Infantas Field, Colombia, Middle Magdalena Basin, in E. A. Beaumont and N. H. Foster eds., Structural Traps VII: Tulsa, AAPG Treatise of Petroleum Geology, Atlas for oil and gas fields, p. 323-347.

Information Handling Services (IHS) Markit, 2010, accessed December 1, 2015, https://www.ihs.com/industry/oil-gas.html.

Mora, A., T. Gaona, J. Kley, D. Montoya, M. Parra, L. Ignacio Quiroz, G. Reyes, and M. R. Strecker, 2009, The role of inherited extensional fault segmentation and linkage in contractional orogenesis: a reconstruction of Lower Cretaceous inverted rift basins in the Eastern Cordillera of Colombia, Basin Research, v. 21, p. 111-137, doi:10.1111/j.1365-2117.2008.00367.x.

Morales, L. G., and the Colombian Petroleum Industry, 1956, General geology and oil occurrences of the Middle Magdalena Valley, Colombia, in L. G. Weeks, ed., Habitat of the middle and upper Magdalena basins, Colombia: Oil—A symposium: AAPG, p. 641-695.

Parra, M., A. Mora, E. R. Sobel, M. R. Strecker, and R. Gonzalez, 2009, Episodic orogenic front migration in the northern Andes: Constraints from low-temperature thermochronology in the Eastern Cordillera, Colombia, Tectonics, v. 28, TC4004, doi:10.1029/2008TC002423.

Prince, M., R. Acevedo, C. Sanchez, and D. Rojas, 2011, Upper Cretaceous in the Middle Magdalena Valley, Colombia, South America: A New exploratory target in an old mature basin: AAPG Search and Discovery, no. 10296.

Ramon, J. C., L. I. Dzou, W. B. Hughes, and A. G. Holba, 2001, Evolution of the Cretaceous organic facies in Colombia: implications for oil composition: Journal of Southern American Earth Sciences, v. 14, p. 31-50.

Rangel, A., P. Parra, and C. Nino, 2000, The La Luna formation: chemostratigraphy and organic facies in the Middle Magdalena Basin, Organic Geochemistry, v. 31, p. 1267-1284.

Rangel, A. J. M. Moldowan, C. Nino, P. Parra, and B. N. Giraldo, 2002, Umir Formation: Organic geochemical and stratigraphic assessment as cosource for Middle Magdalena Basin oil, Colombia: AAPG Bulletin, v. 86, no. 12, p. 2069-2087.

Rangel, A., J. F. Osorno, J. C. Ramirez, J. De Bedout, J. L. Gonzalez, and J. M. Pabon, 2017, Geochemical assessment of the Colombian oils based on bulk petroleum properties and biomarker parameters: Marine and Petroleum Geology, v. 86, p. 1291-1309, doi:10.1016/j.marpetgeo.2017.07.010.

Restrepo-Pace, P. A., F. Colmenares, C. Higuera, and M. Mayorga, 2004, A fold-and-thrust belt along the western flank of the Eastern Cordillera of Colombia—Style, kinematics, and timing constraints derived from seismic data and detailed surface mapping, in K. R. McClay, ed., Thrust tectonics and hydrocarbon systems: AAPG Memoir 82, p. 598-613.

Reyes-Harker, A., C. F. Ruiz-Valdivieso, A. Mora, J. C. Ramirez-Arias, G. Rodriguez, F. de la Parra, V. Caballero, M. Parra, N. Moreno, B. K. Horton, J. E. Saylor, A. Silva, V. Valencia, D. Stockli, and V. Blanco, 2015, Cenozoic paleogeography of the Andean foreland and retroarc hinterland of Colombia: AAPG Bulletin, v. 99, no. 8, p. 1407-1453.

Villamil, Tomas and C. Arango, 1998, Integrated stratigraphy of latest Cenomanian and Early Turonian facies of Colombia, in Pindell, J. L., and C. Drake eds., Paleogeographic evolution and non-glacial eustasy, northern South America: Society for Sedimentary Geology Special Publication 58, p. 129-159.

Villamil, Tomas, 1999, Campanian—Miocene tectonostratigraphy, depocenter evolution and basin development of Colombia and western Venezuela, Palaeogeography, Palaeoclimatology, Palaeoecology, v. 153, p. 239-275.

Zumberge, J. E., 1980, Oil-oil and oil-source rock correlations of bacterially degraded oils and Cretaceous outcrops from Colombia, South America (abs.): International Geological Congress 26, July 7-17, 1980, Paris, p. 806.

Zumberge, J. E., 1984, Source rocks of the La Luna Formation (Upper Cretaceous) in the Middle Magdalena Valley, Colombia, in J. C. Palacas, ed., Petroleum geochemistry and source rock potential of carbonate rocks: AAPG Studies in Geology 18, p. 127-133.

QUANTITATIVE EVALUATION RULES FOR PROGRAMMED PYROLYSIS GREATLY IMPROVE THEIR RELIABILITY

Allegra Hosford Scheirer[1,*] and Kenneth E. Peters[1, 2]
[1]Department of Geological Sciences, Stanford University, Stanford, CA
[2]Also at Schlumberger, Mill Valley, CA
*allegras@stanford.edu

Abstract

Geochemistry data obtained via programmed pyrolysis of geologic samples are widely used in the oil and gas industry because pyrolysis is a quick and inexpensive technique and the data help to characterize both source and reservoir rock intervals. However, the interpretation of such data is made difficult by several limitations. Among many others, these pitfalls include inconsistency between laboratories and carry-over of the free petroleum signal S1 into the generative potential signal S2, which can cause a low-temperature shoulder on the S2 peak and/or very broad S2, thereby rendering the maximum temperature (Tmax) suspect. To help remedy these and other deficiencies, we codified nine quantitative rules for screening programmed pyrolysis data. We refer to these collectively as PARSE: Pyrolysis Analytical Rules for Screening and Evaluation. The PARSE rules are designed to filter an input data set by a predefined series of quantitative criteria, resulting in a final data set of: 1) reliable thermal maturity indicator Tmax; 2) potential source rock intervals; and 3) potential reservoir rock intervals. PARSE can interpret data from a single well or numerous wells (either individually or aggregated). Moreover, the rules are flexible: thresholds within each rule can be adjusted by basin, kerogen type, user experience, or based on patterns observed in the data. More than half of the rules focus on Tmax. Two of the rules identify intervals of possible migrated oil. Finally, several rules activate when values are deemed geologically or operationally implausible. PARSE has been demonstrated on geochemical logs from oil and gas wells, on outcrop samples, on thermally immature source rock data from an entire basin, and on paired Tmax-vitrinite reflectance data to establish a linear relationship between the two thermal maturity parameters. In summary, PARSE greatly improves confidence in programmed pyrolysis data by rejecting spurious values according to a rigorous set of criteria. In the era of big data and machine learning, such pre-processing steps take on more importance than ever before.

2019 Meeting Posters

APPLICATION OF DEEP LEARNING IN SUBSURFACE FAULTS DETECTION WITH SEISMIC DATA

Anatoly Aseev
Department of Geological Sciences, Stanford University, Stanford, CA
aaseev@stanford.edu

EVALUATING STRIKE-SLIP FAULT EVOLUTION WITH LABORATORY EXPERIMENTS AND 2D CONVOLUTIONAL NEURAL NETWORKS

Laainam "Best" Chaipornkaew
Department of Geological Sciences, Stanford University, Stanford, CA
bestc@stanford.edu

UNCONVENTIONAL POTENTIAL OF THE SHUBLIK FORMATION, ALASKA NORTH SLOPE

Allegra Hosford Scheirer
Department of Geological Sciences, Stanford University, Stanford, CA
allegras@stanford.edu

CHARACTERIZATION OF PORE MICROSTRUCTURE AND METHANE ADSORPTION OF BLACK SHALES IN EARLY CAMBRIAN FROM SOUTH CHINA

Yanran Huang
Department of Energy Resources Engineering, Stanford University, Stanford, CA
huangb77@stanford.edu

HOPANE ISOTOPE RATIOS ARE CRITICAL TO DISTINGUISH SIX OIL TYPES AND THEIR MIXTURES IN BRAZIL

Mike Moldowan
Biomarker Technologies Inc., Rohnert Park, CA
jmmolodowan@biomarker-inc.com

FAVORABLE UNCONVENTIONAL RESOURCE POTENTIAL OF THE SHUBLIK FORMATION, CENTRAL NORH SLOPE, ALASKA, USA

Allegra Hosford Scheirer[1,*], Leslie B. Magoon[1], Kenneth J. Bird[2], Edward A. Duncan[3]
[1]*Department of Geological Sciences, Stanford University, Stanford, CA*
[2]*Consultant*
[2]*Duncan Petroleum*
[*]allegras@stanford.edu

Abstract

Favorable potential for the Shublik shale oil play in the Central Alaska North Slope is based on geochemical, physical property, and seismic data acquired over the last several decades. The Alaska North Slope is a world-class petroleum province, with 50 years of production totaling about 15 billion barrels of oil from conventionally trapped accumulations. Despite this success, organic-rich source rocks within the region have yet to be successfully drilled as unconventional plays. This research defines the geochemical and physical parameters that make the Shublik Formation a target for commercial shale oil.

This source rock is regionally extensive, ranges in thickness from 80 to 200 ft (25 to 60 m), and has original organic carbon and hydrogen indices of 2 to 10 wt% and ~700 to ~1000 mg HC/g TOC, respectively. In the area most prospective for shale oil, the thermal maturity of the Shublik Formation ranges from 0.9 to 1.35% R_o. The ability to produce petroleum by artificial stimulation is likely enhanced by natural fracturing, which is observed from hand sample scale to regional seismic scale. Fractures are aligned with the minimum and maximum horizontal stress directions and stress anisotropy is small. Finally, both mineralogy (carbonate and quartz rich, clay poor) and elastic properties (high Young's modulus, low Poisson's ratio) indicate that the Shublik source rock is geomechanically optimal for artificial fracturing. With completion techniques already developed in successful shale oil accumulations, the Shublik Formation should be considered a viable resource play in the Central North Slope in Alaska.

CHARACTERIZATION OF PORE MICROSTRUCTURE AND METHANE ADSORPTION OF BLACK SHALES IN EARLY CAMBRIAN FROM SOUTH CHINA

Yanran Huang[1,2*], Ye Yu[2], and Tapan Mukerji[1]
[1]*Department of Energy Resources Engineering, Stanford University, Stanford, CA*
[2]*Hunan University of Science and Technology, Xiangtan, China, 411201*
[*]huangb77@stanford.edu

Abstract

There is no breakthrough on shale gas exploration in northwestern (NW) Hunan from South China yet. However, the cumulative production of the Fuling shale gas field has reached 1 $\times 10^{11}$ m^3 in recent years, and now Yiye1HF well and Yangye1HF well have respectively 1.24 $\times 10^5$ m^3 and 2.89 $\times 10^5$ m^3 unimpeded production of shale gas per day from early Cambrian formations. The study area has good hydrocarbon generation conditions with a large spatial extent of organic-rich Niutitang black shales. However, this area has experienced a long and strong tectonic deformation, and the ancient reservoirs may have been damaged possibly to the point where they no longer exist. Based on the data of an exploratory well in NW Hunan, the adsorbed state of shale gas accounts for 69.7% on average with a range of 49.8 % to 83.5 %. In comparison, the adsorbed state of shale gas in Fuling field only accounts for an average of 34.3% with a range of 27.1 % to 47.8 %. Therefore, the adsorption abilities of the shale reservoir play a significant role in the success of exploration and production of shale gas. In this paper, wells HY1, CY1 and SY were studied to systematically analyze the feature of pore microstructure and methane adsorption (**Figure 1**).

Until now, there is no unified scheme for the classification of shale pores. We can divide the pores into mineral matrix pores, organic-matter pores and fracture pores under field emission scanning electron microscope (FESEM). These pores can be further classified according to their shape features and formation mechanism (**Figure 2**).

In the two different stages ($0<P/P_0<0.5$ and $0.5<P/P_0<1$, P is the partial pressure of N_2, and P_0 is saturated vapor pressure of N_2 at the experimental temperature), we can get the two different fractal dimension D_1 and D_2 from low temperature N_2 adsorption (**Figure 3a**). The process of N_2 adsorption is governed by Van der Waals force under low pressure, corresponding to fractal dimension D_1. Because of N_2 molecule was adsorbed and arranged on the surface, where surface adsorption dominated, D_1 can reflect the surface roughness of the pore microstructure. Meanwhile, at higher pressure, adsorbed gas increasingly depends on multi-layer adsorption and even capillary condensation, corresponding to fractal dimension D_2, which is used to define the pore microstructure irregularity. There is a significant correlation between D_1 and D_2 in well HY1 and SY, which means the function of pore roughness and irregularity is consistent. Except well CY1, we can find that D_1 has a better relationship with Langmuir volume (**Figure 3b**). Meanwhile, there is no correlation between D_2 and Langmuir volume. It is easy to conclude that the abilities of gas storage are

more dependent upon the surface roughness of the pores, but not the irregularity. There is also a strong positive relationship between ln (TOC) and D_1 (**Figure 3c**), which means that the effect of TOC is more sensitive within a lower range.

The organic matter (OM) pores with kerogen macromolecular aggregation are also widely developed, and they can provide a large special surface area (SSA) and total pore volume (TPV) (**Figure 4a-b**). Meanwhile, OM is the material basis for gas adsorption, and has a strong adsorption ability and ample space for gas storage. There is also a strong positive correlation between TOC and Langmuir volume (**Figure 4c**). Abundant OM is very important to improve gas adsorption capacity of shale reservoir in different ways.

Figures

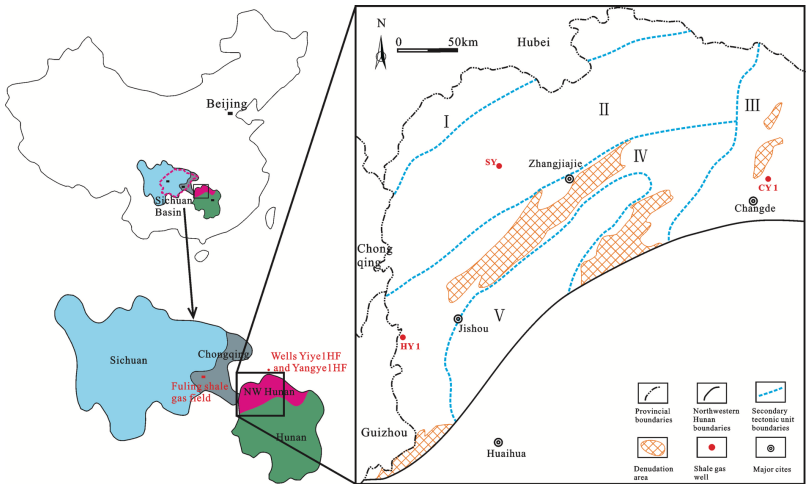

Figure 1. Geographical map of northwestern Hunan and some shale gas wells.

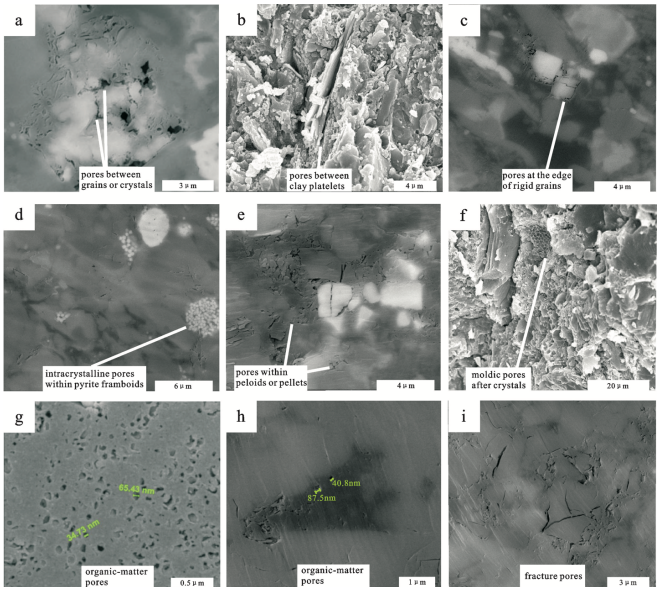

Figure 2. The microstructure features of different pores under FESEM.

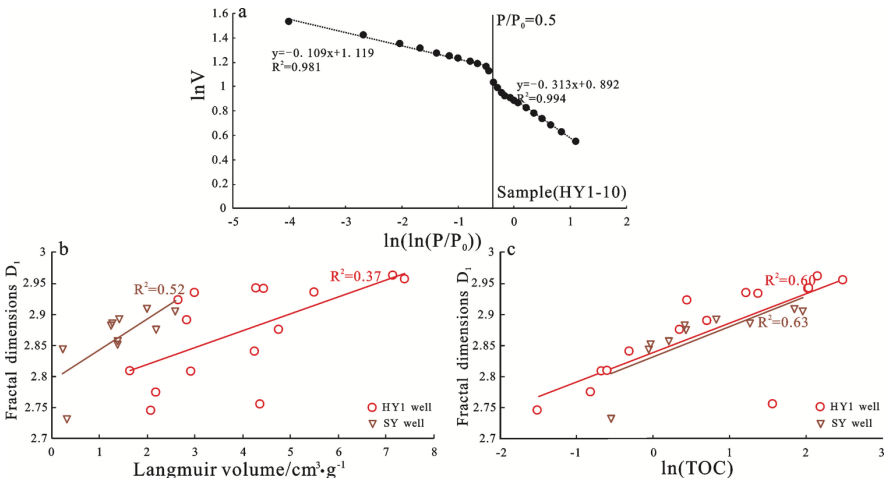

Figure 3. The results of low temperature N_2 adsorption.

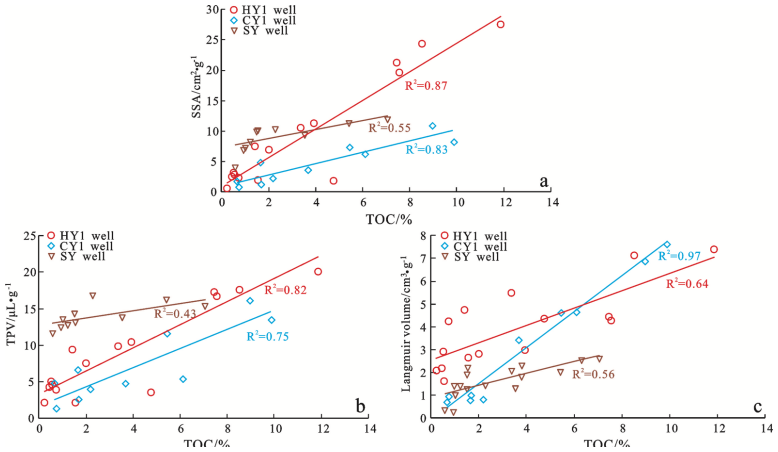

Figure 4. Correlation between TOC and SSA, TPV, and Langmuir volume.

Acknowledgments

The authors would like to thank the foundation of National Natural Science Foundation of China (No. 41603046) and the Natural Science Foundation of Hunan province (No. 2019JJ50178). The author Yanran Huang also acknowledges the support of the program of China Scholarships Council (No.201809480006).

References

Borjigin T, Shen BJ, Yu LJ, et al. (2017) Mechanisms of shale gas generation and accumulation in the Ordovician Wufeng–Longmaxi formation, Sichuan basin, SW China. Petroleum Exploration and Development 44(1): 69–78.

Curtis JB (2002) Fractured shale-gas system. AAPG Bulletin 86(11): 1921–1938.

Saidian M, Godinez LJ and Prasad M (2016) Effect of clay and organic matter on nitrogen adsorption specific surface area and cation exchange capacity in shales (mudrocks). Journal of Natural Gas Science and Engineering 33: 1095–1106.

Loucks RG, Reed RM, Ruppel SC, et al. (2009) Morphology, genesis and distribution of nanometer-scale pores in siliceous mudstones of the Mississippian Barnett shale. Journal of Sedimentary Research 79(11/12): 848–861.
Wang SQ. (2017) Shale gas exploration: status, issues and prospects. Natural Gas Industry 37(6): 115–130.

HOPANE ISOTOPE RATIOS ARE CRITICAL TO DISTINGUISH SIX OIL TYPES AND THEIR MIXTURES IN BRAZIL

J. M. (Mike) Moldowan[1,*], Jeremy E. Dahl[2] and Marcio R. Mello[3]
[1]*Biomarker Technologies, Inc., 638 Martin Avenue, Rohnert Park, CA, USA*
[2]*Stanford University, Stanford Inst. for Materials and Energy Sciences, Geballe Laboratory for Advanced Materials*
[3]*Brazil Petrostudies, Rio de Janeiro, Brazil*
*jmmoldowan@biomarker-inc.com

Abstract

Compound specific isotope analysis of biomarkers/hopanes (CSIA-Bh) is a powerful method for correlation of crude oils and determination of their sources. As many as six source rock depositional environments are delineated for oils in the Brazilian margin by CSIA-Bh. By using "end-member" oil samples related to the six sources originally determined by geological considerations and biomarkers it was determined that the oils generated from each of them show unique hopane isotope ratio trends. The hopane isotope ratios for the different oil types cover a range from about -17 to -51 ‰, extending the known isotope-ratio-range for any compounds ever reported from petroleum. The sources of co-sourced oil can be determined by concomitant use of both CSIA-Bh and advanced analysis of large diamondoid molecules (i.e., QEDA, see Moldowan, et al., 2015)

Interpreting Hopane Isotope Ratios in Crude Oil

Hayes et al. (1990) suggested a model for water column stratification and chemistry that could produce a great diversity of isotopic variations in biomarkers. In Figure 1 we show an array of variations in hopane isotope ratios obtained from Brazilian oil samples by CSIA-Bh using segregated hopane fractions. Based on analysis by gas chromatography-mass spectrometry-mass spectrometry (GC-MS-MS) of biomarkers and other geochemical data and geological inferences the hopane isotope ratio trends have been linked to certain depositional environments found to have occurred in the Brazilian basins. In line with the Hayes model, one might suppose that the isotopically lightest hopanes have been contributed by methanotrophs using methane as a carbon source and that a stable stratified water column facilitated the process. It is interesting to note that ^{13}C depletion is strongest for 30-norhopane (down to -51 ‰) suggesting origins dominated by different bacteria compared with the higher hopane homologs in the same oil sample, which can be as much as 12 ‰ heavier. In contrast, relatively heavy (up to -17 ‰) and virtually flat C-isotope trend lines are observed for some oil samples generated from marine source rocks. Such distributions suggest those hopanes were produced predominantly by cyanobacteria using relatively heavy CO_2 for photosynthesis in a water system where a significant stable stratification to full anoxia had not occurred.

It is also interesting to note the C-isotope ratios for gammacerane are as much as 23 ‰ heavier than that of 30-norhopane in the same oil sample. The bacterivorous ciliates that produce the proposed precursor of gammacerane, tetrahymanol (Damsté et al., 1995),

must *not* be feeding primarily on those bacteria that produced the preponderance of the isotopically light hopanes in the same water systems.

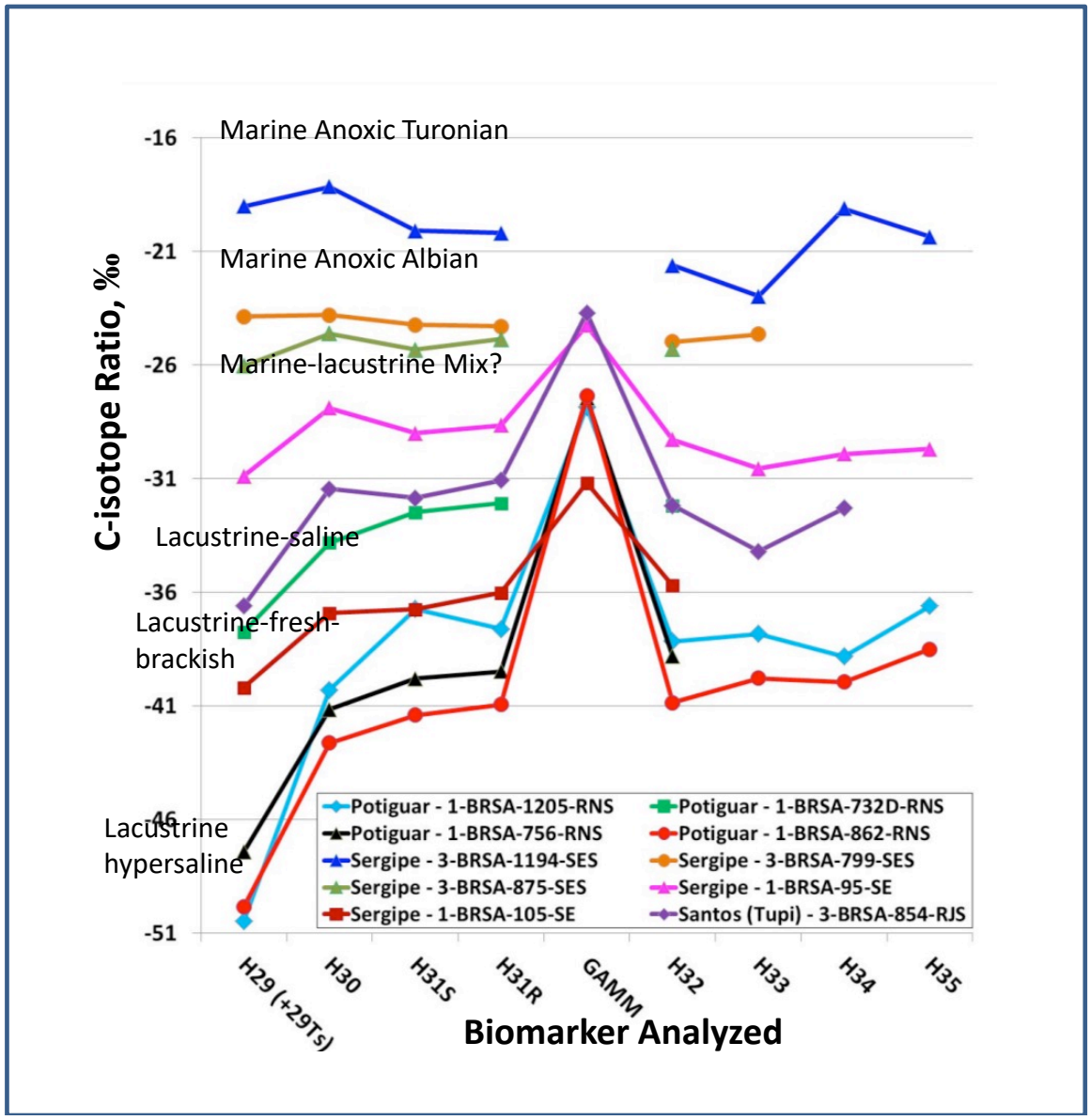

Figure 1 Applications of compound specific isotope analysis of biomarkers/hopanes (CSIA-Bh) for end-member oil samples from fields in the Brazil Atlantic Margin. The wide range of hopane isotope ratios obtained from these oil types can be applied to determine the source of any oil having sufficient hopanes to make the CSIA measurement. The hopanes must first be segregated by a combination of liquid chromatography and adsorption and release from a variety of zeolites in order to obtain fractions pure enough for isotope ratio measurements by gas chromatography-isotope ratio mass spectrometry (GC-IRMS). CO_2 recycled in an anoxic water column results in depletion of the ^{13}C relative to ^{12}C and isotopically heavy CO_2 which, when used as a carbon source for anaerobic bacteria can result in isotopically light hopanes. Oils from source rocks deposited in lacustrine

hypersaline depositional environments show extremely light C_{29}-hopane which is believed to derive from the use of biogenic methane as a carbon source for methanotrophs. A deep stable highly anoxic zone in a stratified water column may segregate and preserve the hopanes coming from anaerobic bacteria from those of cyanobacteria, which can be reworked and re-oxidized near the top of the water column.

References

Damste, J.S.S., et al. (1995) *Geochim. Cosmochim. Acta* 59, 1895-1990.

Hayes, J.M., et al. (1990) *Org. Geochem.* 16, 1115-1128.

Moldowan, J.M., et al. (2015) *J. Petroleum Science & Engineering* 126, 87-96.

NOTES